OBSERVATION AND INTERPRETATION OF LUNAR OCCULTATIONS

BY

RICHARD RAEBURN RADICK

B.A., University of Minnesota, 1969
M.S., Rensselaer Polytechnic Institute, 1973

THESIS

Submitted in partial fulfillment of the requirements
for the degree of Doctor of Philosophy in Astronomy
in the Graduate College of the
University of Illinois at Urbana-Champaign, 1978

Urbana, Illinois

OBSERVATION AND INTERPRETATION OF LUNAR OCCULTATIONS

BY

RICHARD RAEBURN RADICK

B.A., University of Minnesota, 1969
M.S., Rensselaer Polytechnic Institute, 1973

THESIS

Submitted in partial fulfillment of the requirements
for the degree of Doctor of Philosophy in Astronomy
in the Graduate College of the
University of Illinois at Urbana-Champaign, 1978

Urbana, Illinois

Acknowledgments

To Mark Nelson, who introduced me to high-speed, high-resolution photoelectric astronomy, and has guided and encouraged my research efforts for some four years; to Michael Faiman, who provided valuable guidance during the design of the observational system upon which this dissertation rests; to John Dickel, who adopted me as an "orphaned" graduate student, and provided support for part of this research through NASA Grant NGR14-005-176; to John Gallagher, who undertook the task of directing my thesis research during its final stages, I owe special debts of gratitude. Special acknowledgment and thanks are also due to the members of the suppport staff of Prairie Observatory, who assisted in the realization of my various design schemes, and to my fellow graduate students, the "Basement Crew" of the Observatory, a roguish bunch among whom I have spent five memorable years.

Table of Contents

List of Tables

List of Figures

I. Introduction

1.1 Terminology

This dissertation will consider the observation and interpretation of lunar occultations. Broadly speaking, an occultation is any eclipse in which the apparent size of the eclipsing body is much larger than that of the eclipsed body. Because of its relatively large angular size and rapid motion, most occultations involve the moon as the eclipsing body. Any event of this sort is called a "lunar occultation."

The inclination of the moon's orbital plane relative to the ecliptic, the regression of the nodes of its orbit, and geocentric parallax combine to ensure that any object lying within some 6½ degrees of the ecliptic will be occulted by the moon at some time for some observer. These objects include a representative sampling of the entire list of common astronomical objects. Thus, the term "lunar occultation" embraces a wide variety of phenomena.

Lunar occultations have been observed and recorded visually since antiquity, and by means of optical, infrared, and radio detectors in modern times. In this dissertation the term "observation" will generally indicate the use of modern photoelectric detectors operating in the visual region of the spectrum (roughly 3500 Å to 10000 Å).

In the visual region, competition from moonlight scattered by the Earth's atmosphere hampers the observation of occultations involving faint or diffuse objects. Therefore, the great majority of photoelectrically observable lunar occultations involve stars brighter than about 9th magnitude. All the planets except Pluto, as well as the

brighter satellites and asteroids, are also included among the observable objects. Besides this "standard fare," an occasional comet or globular cluster might also attract the interest of an occultation observer. Typically, perhaps ten occultations involving observable stars occur during the course of a single night, two or three events each month involve a star brighter than 6th magnitude, and two or three observable solar system objects are occulted each year, for any one observer.

1.2 Occultation Observations: Timings

Until recently, observing a lunar occultation has meant timing the contact. Since the moon has no appreciable atmosphere, an occultation occurs very rapidly: a star seems to disappear (or reappear) almost instantaneously.

Occultation timings provide precise information about the relative locations of the observer, the moon, and the occulted object. This fact has been recognized and exploited by astronomers since the earliest times. Ptolemy, for example, used occultation records extending over several centuries to calculate a numerical value for the precessional period of the equinoxes (The Almagest, Book VII). In modern times, occultation timings have found a variety of uses in geodesy, celestial mechanics, and timekeeping.

One important former geodetic application for occultation timings was the determination of longitude (e.g., Chauvenet, 1868). The introduction of radio time signals has rendered this particular application obsolete. However, occultation timings have continued to

find some geodetic uses in recent years - for example, in the study of the detailed figure of the Earth (O'Keefe and Anderson, 1952).

In celestial mechanics, occultation timings, through their ability to accurately measure the position of the moon relative to the stellar background, have provided a means for verifying the predictions of lunar theory and improving the constants of lunar motion. A visual observer can time an occultation accurately to 0.2 second, which fixes the location of a point on the lunar limb to about 0.10 arcsecond, or 200 meters. Modern photoelectric observations can yield timings accurate to 0.001 second, implying positional accuracy comparable to that obtainable by laser ranging techniques.

The gravitational time scale known as Ephemeris Time is based largely on the observation of lunar motion, which, in turn, relies heavily on occultation timings. Timings are also one of the chief sources of data relating Ephemeris Time to Universal Time.

The accuracy of a timing depends, of course, on the technique used to obtain it. However, it is irregularities in the shape of the lunar limb, rather than timing errors, which currently limit the accuracy of inferences based on occultation timings: the relationship between any point on the lunar limb and the center of the moon is uncertain by some tens of meters (Watts, 1963). In anticipation that improved lunar limb corrections may eventually become available, modern photoelectric occultation observers have informally adopted a standard of 0.001 second for the precision of their timings (Nather and Evans, 1970; Schlosser et al., 1970; Eitter and Beavers, 1974). If limb corrections accurate to one meter were to become available, such timings could perhaps be

used for the determination of trigonometric parallaxes (Nather and Evans, 1970).

1.3 Occultation Observations: High-resolution Astrometry

The introduction of modern photoelectric techniques has led to much more than just a substantial improvement in the accuracy of occultation timings. High-speed photoelectric detectors are capable of following the details of an occultation light curve, and this ability has had a profound effect on high-resolution astronomy. Today, lunar occultations provide the only means whereby a single telescope can achieve an angular resolution greatly exceeding its diffraction limit. For example, a one-meter telescope has a diffraction limit of about 0.1 arcsecond, according to the Rayleigh criterion. The same telescope, equipped with an appropriate data recording system and used to observe lunar occultations, can detect structures with angular sizes as small as 0.002 arcsecond. Furthermore, the resolution obtainable through occultation techniques does not depend critically on the imaging ability of the telescope, which is seriously degraded by atmospheric seeing effects.

The moon occults perhaps 100 stars which show angular diameters larger than 0.002 arcsecond. These stars represent the largest group of stars accessible to any current technique capable of resolving a stellar disk. In addition, occultation observations have proven extremely useful for the discovery and resolution of close multiple star systems, and permit accurate relative photometry of these stars as well.

Unfortunately, the appreciation and exploitation of these capabilities has been a slow process. MacMahon (1909) first proposed

that occultation observations could be used to directly measure the angular sizes of stars, and estimated that a star 0.001 arcsecond in diameter should take some 0.002 second to be occulted. Eddington (1909) promptly replied that MacMahon had neglected diffraction effects in his estimate, that the measured interval would characterize the diffraction pattern and not the star (except for a few stars showing very large disks), and that occultation measurements could not, therefore, be of much use for resolving stars.

This stinging rebuttal apparently discouraged further inquiry into the problem for thirty years, until Williams (1939) pointed out that, although the angular size of the source, indeed, does not appreciably affect the time scale of the diffraction pattern, it does alter the relative amplitudes of the diffraction fringes. He also suggested that photoelectric techniques could be used to trace the fringe pattern, and concluded that stellar diameters as small as 0.004 arcsecond could be measured in this fashion.

In fact, Whitford (1939) was, at that very time, engaged in making photoelectric tracings of occultation diffraction patterns. On 6 September 1938 and 7 September 1938 he observed occultations of β Capricorni and ν Aquarii, respectively, with the Hooker telescope at Mount Wilson. Using the amplified output of a photocell to drive the vertical deflection plates of an oscilloscope, he made a motion picture of the display. Only the light curve of β Cap was analyzed in detail. Whitford did not feel that he had resolved the disk of this star, although he did claim that a diameter larger than 0.002 arcsecond would be above the detection threshold of his technique (in fact, the star has

an angular diameter of almost 0.004 arcsecond, but this does not diminish Whitford's observational achievement). He also noted that the time scale of the observed diffraction pattern implied a slope of 7.6 degrees on the lunar limb at the point of occultation.

By 1946 Whitford claimed to have measured two angular diameters (Whitford, 1946). However, the first indisputable resolution seems to have been obtained in the early 1950's by several workers in South Africa (Evans, 1951; Cousins and Guelke, 1953; Evans et al., 1954). The star was Antares (α Scorpii).

Anomalies in one of these observations helped spark a controversy over the effect lunar limb irregularities might have on occultation measurements. Eddington (1909) had already pointed out that limb obstacles the size of the first Fresnel zone ($\sim$10 m) could affect the shape of the fringe pattern. Detailed calculations now demonstrated that the distortions could be dramatic indeed (e.g., Evans, 1970; Morbey, 1972). This concern, the success of the intensity interferometer in resolving stars (Brown, 1968), the technical demands imposed by occultation observations, and the complicated nature of the data analysis all conspired to further delay the exploitation of occultation techniques.

In late 1968, a systematic program to observe lunar occultations was undertaken at the McDonald Observatory of the University of Texas. By 1970, sufficient evidence was available from this program, Lunar Orbiters, and Apollo landings to argue convincingly that the lunar limb is comparatively free from the irregularities that had so preoccupied the discussions of the previous fifteen years. Simultaneously, the

introduction of computer technology eased the problems of data acquisition and analysis, and it became both feasible and attractive for observatories with modest facilities to undertake photoelectric lunar occultation observing programs. Today, programs for routinely observing occultations exist at the Fick Observatory of Iowa State University and the Hamburg Observatory, as well as at the McDonald Observatory. Other observatories, notably the Kitt Peak National Observatory, are concentrating on observing events of special interest.

1.4 Outline of the Remainder of the Dissertation

The remainder of this dissertation describes an effort to construct a system for observing lunar occultations at the Prairie Observatory of the University of Illinois, and the analysis of some of the observations obtained with it during the calender year 1977. Much of this program has built upon the efforts of an earlier worker, Dr. Mark Nelson.

The following section presents a detailed picture of the occultation process. Particular attention is paid to the constraints the process places on any observational system which hopes to successfully record occultation events. A description of the design and operation of the data-recording system which has been constructed for use at Prairie Observatory is then given.

Following these discussions is an analysis of observational results. A summary of observations is presented, followed by the analysis of a major stellar event, the 20 October 1977 occultation of β Capricornii. The 10 February 1977 occultation of the planet Uranus is then considered. The dissertation concludes with an assessment of the

"Page missing from available version"

II. The Occultation Process

2.1 Preliminary Description

As the moon occults a star, it casts a faint shadow which moves across the surface of the Earth at a rate which, although varying from event to event, can be as much as about 0.9 km/sec. The edge of this shadow is modified by diffraction at the lunar limb into a series of fringes. A fixed telescope observes the occultation as rapid variations in the light level as this fringe pattern sweeps across its aperture. A photoelectric observation of the event consists of a time record of these intensity fluctuations.

2.2 Fresnel Theory: The Monochromatic Point Response

A lunar occultation may be idealized as Fresnel diffraction by a semi-infinite plane bounded by a sharp straight edge. (e.g., Born and Wolf (1970). The treatment presented here is well-known and standard. The particular notation follows closely that used by S.D. Tremaine at Princeton.)

Referring to Figure 1, let

r' be the distance to the source S,

s' be the distance to the observer O, and

Io be the intensity as $x \to \infty$.

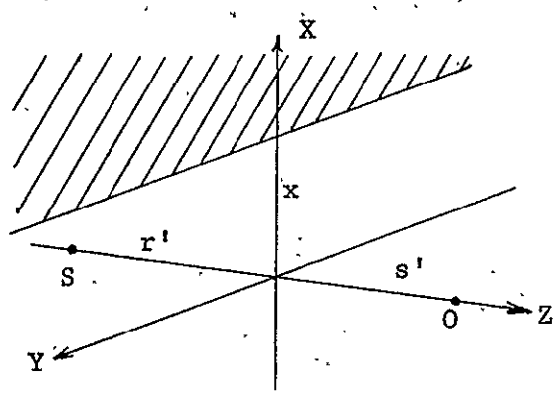

Figure 1 Straight Edge Geometry

Then

$$I(x) = \frac{I_0}{2}\left[\left(\frac{1}{2} + C(w)\right)^2 + \left(\frac{1}{2} + S(w)\right)^2\right]$$

where

$$C(w) = \int_0^w \cos\left(\frac{\pi}{2}\tau^2\right) d\tau$$

and

$$S(w) = \int_0^w \sin\left(\frac{\pi}{2}\tau^2\right) d\tau$$

are the Fresnel integrals, with

$$w = \sqrt{\frac{2}{\lambda}\left(\frac{1}{r'} + \frac{1}{s'}\right)}\, x \ .$$

For lunar occultations, $r' \to \infty$ and $s' = D$, the lunar limb distance, and

$$w = \sqrt{\frac{2}{\lambda D}}\, x \ .$$

Alternatively,

$$I(x) = \frac{I_0}{\lambda D}\left[\int_{-\infty}^{x} \exp\left(\frac{i\pi y^2}{\lambda D}\right) dy \cdot \int_{-\infty}^{x} \exp\left(\frac{-i\pi y^2}{\lambda D}\right) dy\right] .$$

Since time is a more convenient variable, let $x = -vt$, where $-v$ is the shadow velocity (negative for disappearances). Define

$$p(\lambda, t) = I(-vt) = \frac{I_0}{2}\left\{\left[\frac{1}{2} - C\left(\sqrt{\frac{2}{\lambda D}}\, vt\right)\right]^2 + \left[\frac{1}{2} - S\left(\sqrt{\frac{2}{\lambda D}}\, vt\right)\right]^2\right\}$$

or

$$p(\lambda, t) = \frac{I_0}{\lambda D}\left[\int_{vt}^{\infty} \exp\left(\frac{i\pi y^2}{\lambda D}\right) dy \cdot \int_{vt}^{\infty} \exp\left(\frac{-i\pi y^2}{\lambda D}\right) dy\right] .$$

The function $p(\lambda,t)$ represents the intensity as a function of time for the disappearance of a monochromatic point star behind the lunar limb, as observed through a point aperture.

It may be rightly objected that the lunar limb is not a sharp straight edge - that it has both depth along the line of sight and detail across it. However, it appears that neither fact is of much practical concern. Murdin (1971) has analyzed the problem of structure along the line of sight and concludes that, at worst, it alters the Fresnel pattern so as to produce timing errors on the order of microseconds and amplitude modifications on the order of one part in ten-thousand. Such effects are of no practical consequence. Similarly, structures across the line of sight which could seriously distort the fringe pattern appear to be relatively uncommon, as has already been mentioned, and therefore are also of little practical concern.

2.3 The Occultation Time Scale and its Implications

Before discussing the factors which modify the point response, the time scale for occultation events should be considered more closely, as this represents one of the principal constraints to the design of an observing system.

The rate at which the lunar limb advances across the occulted object (the shadow velocity) depends on the velocity of the moon in its orbital motion about the Earth, the reflected velocity of the observer due to the Earth's rotation, and the geometry of the event. Orbital motion contributes about 0.9 km/sec. Reflected velocity, for an observer at the equator observing the moon at the zenith, is slightly

less than 0.5 km/sec. The reflected velocity vanishes as the moon moves toward the horizon. Consequently, the difference between the orbital and reflected velocities, which represents the apparent velocity of the moon's center, varies between about 0.4 km/sec and 0.9 km/sec. The effect of geometry is illustrated in Figure 2. If v_o is the apparent lunar velocity and φ the contact angle as defined in the figure, then the shadow velocity is

$$V = V_o \cos(\varphi) ,$$

neglecting local slopes. If there is a local slope θ, defined in the sense shown in the figure, the shadow velocity becomes

$$V = V_o \cos(\varphi - \theta) .$$

It is readily apparent that the time scale for lunar occultations can vary considerably from event to event. Naturally, the design of an observing system must provide for the "worst-possible" case. This case is illustrated as Figure 3, which shows the function $p(\lambda=5500\text{Å},t)$, calculated for a shadow velocity of 0.9 km/sec and a limb distance of about 363000 km. The abscissa of the figure is scaled in milliseconds and the ordinate is normalized such that the undisturbed intensity is unity. Clearly, the spectrum of the diffraction pattern will contain frequencies on the order of a kilohertz. Consequently, the detection system must have a cutoff frequency not significantly less than this if it is to faithfully follow the details of the pattern. In other words, the data-recording system must provide a time resolution of about one

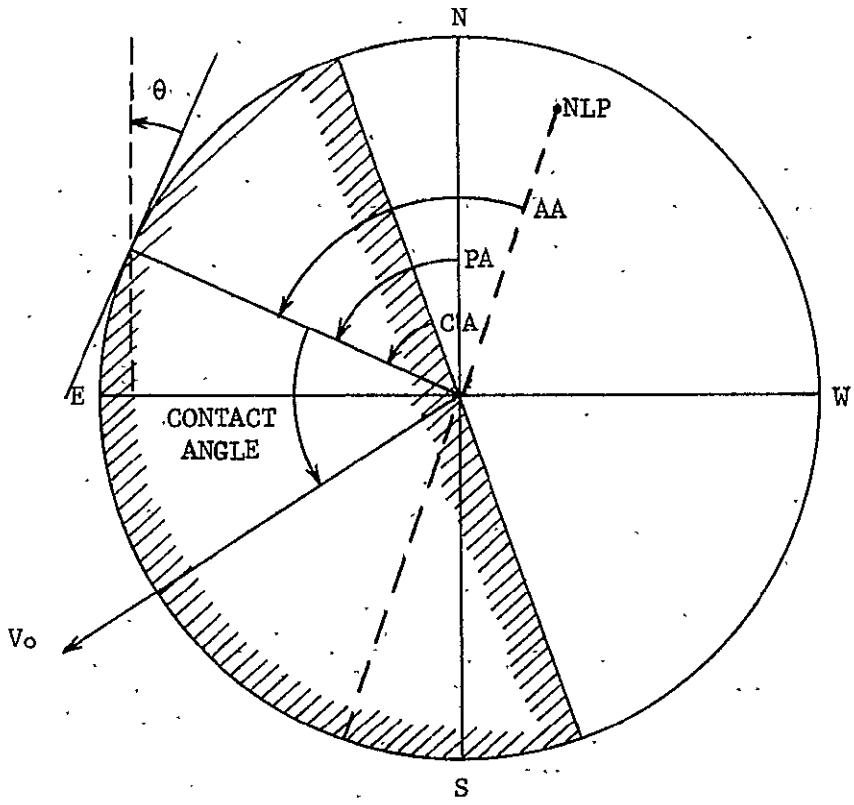

CA = cusp angle
PA = position angle (in sky).
Contact Angle = angle between the point of occultation and the velocity vector
θ = local slope = angle between the true limb profile at the point of contact (dashed line) and the ideal profile (solid line), which assumes a circular limb.
AA = axis angle = angle between the point of occultation and the lunar rotation axis (NLP = north lunar pole).
WA = Watts' angle = AA + 0.22 degrees (Van Flandern, 1970).

Figure 2
Occultation Geometry: Definitions of Angles

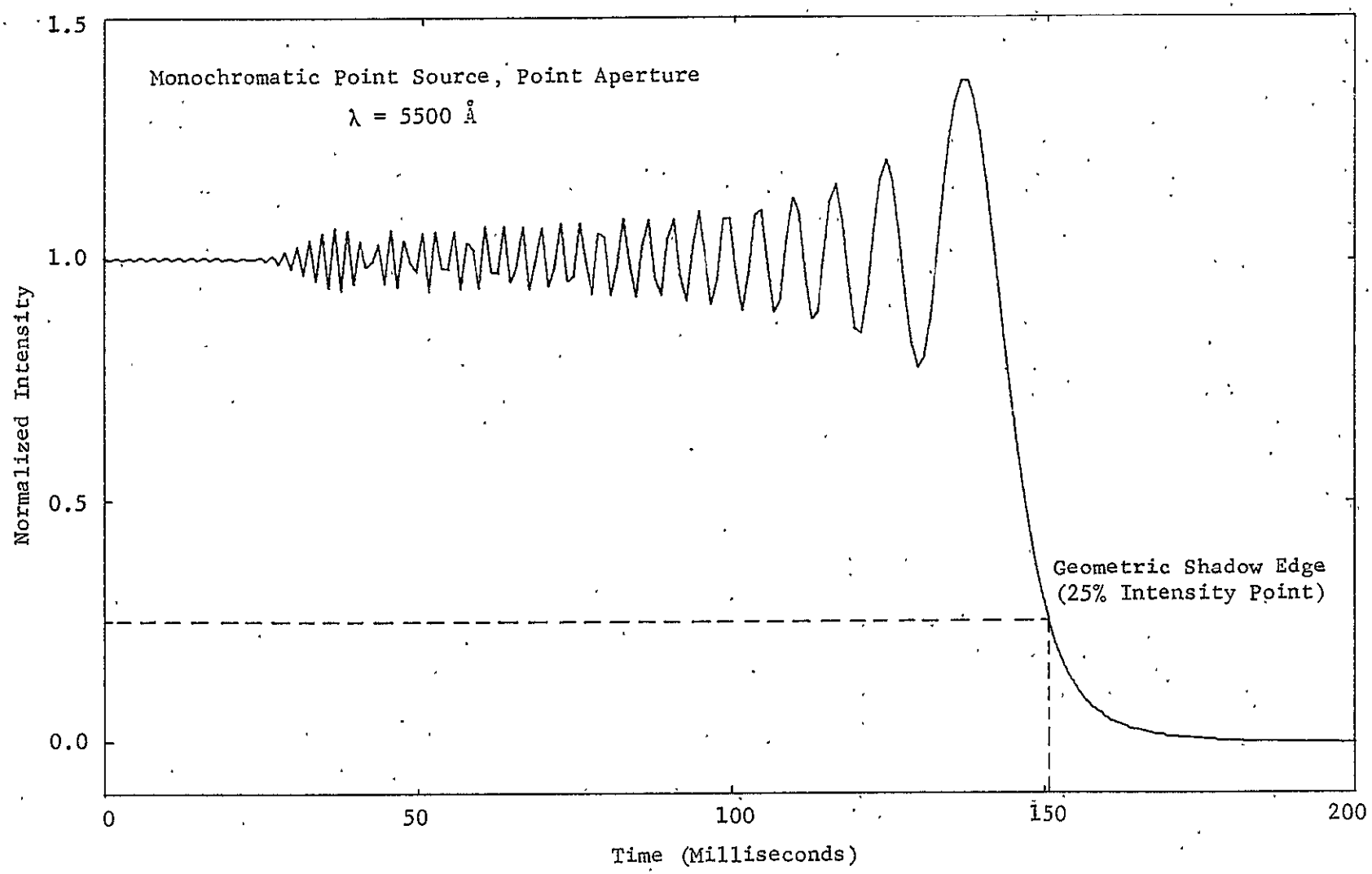

Figure 3 The Function $p(\lambda,t)$

millisecond. It must also be capable of maintaining this data rate over an interval of several seconds, since the exact instant of occultation cannot be accurately predicted.

2.4 The Effects of Aperture, Optical Bandpass, and Source Geometry

For the occultation of a star of finite angular diameter, observed with a telescope of finite aperture through a finite optical bandpass, the intensity observed as a function of time is specified by the relation

$$I_1(t) = \int p(\lambda,t) * a(t) * d(t)\, d\lambda + b ,$$

where

$p(\lambda,t)$ is the monochromatic intensity function defined previously,

$a(t)$ is the strip aperture of the telescope, appropriately normalized,

$d(t)$ is the strip brightness of the source, also normalized, and

b is the lunar background, assumed constant over the interval of interest.

Here "*" represents convolution: $g(t) * h(t) \equiv \int_{-\infty}^{\infty} g(z)\, h(t-z)\, dz$

If a double star is occulted, the observed intensity will be the superposition of two such single star intensity patterns, offset in

time.

The effect of finite telescope aperture on the point response is the smoothing one of convolution. The effect of finite optical bandpass, while not that of a true convolution, is somewhat similar. Each monochromatic component has its own characteristic amplitude and fringe spacing, with the different components sharing as a common origin the geometric shadow edge (the 25% intensity point). Their superposition results in a smoothing of the fringes through cancellation which becomes progressively more complete as the separation from the geometric edge increases.

These two effects create a problem for the photoelectric observer. In order to improve the signal-to-noise ratio of the observation, which depends largely on counting statistics (i.e., the signal-to-noise is proportional to the square-root of the count rate), one would like to maximize the count rate by using a large aperture and a wide optical bandpass. But this would tend to mask those features in the diffraction pattern which are affected by source geometry. Consequently, a compromise must be made. The decisions are complicated by the lunar background, which represents a significant fraction of the total incoming light, and the presence of scintillation noise in the starlight (amplitude distortions caused by atmospheric turbulence). Both of these contributions to the noise vary considerably from observation to observation. Therefore, the optimization problem with respect to signal-to-noise is not very well defined, and cannot be solved uniquely (Nather and Evans, 1970; Ridgway, 1977).

Nonetheless, the effects of aperture, optical bandpass, and time

resolution on angular resolution should be considered. Ridgway (1977) has furnished convenient formulae indicating the limiting resolution associated with each constraint:

aperture a: $\varphi \approx 1.1\ a$ (a in meters)

optical bandpass $\Delta\lambda$: $\varphi \approx 0.107(\Delta\lambda)^{\frac{1}{2}}$ ($\Delta\lambda$ in Ångstroms)

detector resolution Δt: $\varphi \approx 0.443\ \Delta t$ (Δt in milliseconds)

In each case φ, the limiting resolution, is expressed in milliarcseconds.

These constraints indicate that one milliarcsecond angular resolution requires a telescope aperture no larger than about one meter, an optical bandpass no larger than about 100 Å, and a time resolution of at least two milliseconds, to use convenient figures.

2.5 Spectral Filter Selection

Although the width of the optical bandpass has been constrained, the choice of center wavelength remains free. This choice will be influenced by several considerations - the purpose of the observation, the energy distribution of the occulted object, and the sensitivity of the detector being chief among these.

If the objective of the observation is to resolve a single star,

one need not normally use a "standard" spectral filter. Most stars showing a measurable disk are comparatively cool objects, with energy distributions which peak near 10000 Å. The spectral sensitivity of the available detector may force the selection back somewhat toward shorter wavelengths. The infrared absorption bands of atmospheric water vapor should be avoided. The amount of scattered moonlight decreases, and the time scale of the diffraction pattern expands, as one proceeds further into the infrared. Allowing for all these factors, an optical bandpass centered near 7900 Å would appear to be well-suited for an observation of this sort, if an RCA C31034A or other photomultiplier tube with good near infrared sensitivity is used as the photodetector.

If an occultation of a multiple star is being observed, somewhat different considerations apply. Since such observations yield the intensity ratio of the component stars, it is normally desirable to use some "standard" photometric filter, or one which can be easily converted to a standard system. Generally, this indicates the use of the Strömgren four-color filters (or, perhaps, for fainter stars, the Johnson UBV filters). The exact choice will depend, in part, on the spectral types and luminosities of the component stars, if known. For example, one might choose to observe an occultation involving a cool, luminous primary and a hotter, less luminous secondary at short wavelengths, in order to minimize the contrast between the two components.

III. System Design and Operation

3.1 Description of Hardware Resources

The design of any observing system depends, naturally, on available equipment and budget, as well as the constraints imposed by the intended observations. In this case the equipment available consists of a one-meter reflecting telescope, a single-channel Cassegrain photometer for this telescope incorporating a cooled RCA C31034A photomultiplier tube as its photodetector, a high-speed pulse-counting electronic system, and a Texas Instruments Model 960A minicomputer which communicates with the pulse-counting system.

Associated with the computer is a full-duplex teletype of standard design, a Kennedy Model 1600/360 Incremental Magnetic Tape Recorder, and a remote console which allows the observer to control the computer from the telescope. The computer contains 8k of 16-bit memory, about half of which is occupied by the executive program and the service routines for the various system devices. Device interrupts are assigned priorities by the software. The normal priority sequence is: pulse accumulators (highest), TTY printer-punch, TTY keyboard-reader, MTU, and remote console (lowest). The computer also has available to it the readouts from the observatory UT and LST clocks, to 0.1 second resolution. Currently, the UT clock may be set directly from the WWV time signals.

The tape drive operates as a write-only unit, at an incremental data rate of 400 bytes/sec, or at a continuous data rate of 1000 bytes/sec. The incremental write mode is under interrupt control from

the computer, the 400 Hz interrupt signal being supplied by the MTU-CPU interface. In continuous write mode, the tape drive "takes over" the system entirely, blocking interrupts from all other devices until the data transfer is completed.

The high-speed pulse-counting system has two channels, each of which includes an accumulator incorporating a twelve-bit counter and a storage register which is parallel-loaded from the counter by clock pulses derived from a frequency-standard oscillator. The clock pulse interval is adjustable, but one millisecond is normally used. The clock pulses also clear the counters, issue an interrupt to the CPU, and set a "Data Available" flag. Upon responding to the interrupt, the CPU reads and resets the two data registers and the flag (for single-channel operation, only one of the two readings is meaningful - the other is simply discarded). Two other conditions also produce interrupts and set identifying flags: (1) Overflow and (2) Lost Data. "Lost Data" occurs if, for some reason, the CPU does not service the accumulators before the next clock pulse arrives. The design bandwidth of the amplifier-discriminator-accumulator portion of this system is 21 MHz, which is easily adequate for occultation observations.

3.2 The Design Problem, and a Previous Attempt to Solve it

The observational constraints have already been discussed. The two of immediate concern are (1) time resolution of about one millisecond and (2) the ability to operate continuously for several seconds, at least, or, preferably, for about one minute.

The hardware as described above is not well suited for occultation

observations. The time resolution is available but the data storage and/or transfer ability is not. Simply filling the available 4k of computer memory with data is unsatisfactory, since this would allow a run time of only about 4 seconds, which is much too short: occultations are likely to be missed. Transferral of data to tape in incremental write mode encroaches on the necessary time resolution. A data rate of 400 bytes/sec is scarcely adequate for single-channel operation. Should dual-channel operation be desired, it would clearly be too slow. Continuous write mode is not available, since it requires that the CPU ignore the accumulators during transfer.

The first attempt to address this problem (by Mark Nelson) made use of an idea which has also been adopted at the University of Texas, that of a circulating data buffer. Such systems operate by replacing the oldest datum in storage by the one incoming. They require the intervention of either the observer or some automatic level-change detector in order to stop them at the proper time - after the occultation has occurred but before the relevant data has been overwritten. Since a circulating buffer must either reside in the memory of a computer or incorporate a hardware multiscaler of some sort, it has a fairly high cost/data word. Consequently, the length of the buffer is typically quite short. This is no inconvenience for the observation of single stars, but multiple star events may not be observable if the component occultations are much separated in time. The Illinois experience with this arrangement was not particularly encouraging, and, after one success (Nelson, 1975) and several failures, it was abandoned. The Texas version has apparently been more

successful. The difference may be one of site quality. Prairie Observatory suffers from a comparatively severe scintillation problem, and this may have prevented a truly successful utilization of an automatic level-change detection system.

3.3 Design Features of the New Observational System

While thinking about these problems, it occurred to me that if the hardware could be reconfigured so that the tape drive could operate in continuous write mode while the pulse accumulators were active, the benefits of a long continuous run time could be obtained without any sacrifice in time resolution. In continuous mode, the tape drive uses its own 1-kHz oscillator to control the writing process. If this oscillator were made to furnish interrupts to the computer CPU independently from those furnished by the accumulators, the data input and output processes could, in principle, be made to proceed independently and simultaneously.

It was not immediately clear, however, whether or not such a scheme would work at all. The 960A is not a particularly fast machine; typical instruction execution times are of order 4 microseconds. The executive program would have to service two interrupt streams arriving at the rate of 1000/sec on different priority levels and still leave sufficient time to process the incoming data and output it to the tape drive. Calculations showed that, in this interrupt environment, about half of the CPU time is spent in the executive program responding to interrupts. This means that the input-output segments must not have a combined length of more than about 100 instructions if they are to be

successfully executed in the remaining time. This condition is somewhat restrictive, but not excessively so (the combined length of the segments in the current version of the program is about 50 instructions).

The hardware modifications needed to channel the MTU oscillator pulses to the computer as interrupts turned out to be trivial. A three-position switch was installed in the MTU-CPU interface, and some wires were rearranged. The tape drive remains usable in the two original writing modes.

With feasibility established, the remaining features of the design may be considered.

(1). Detailed consideration of the operating requirements of the tape drive indicates that the MTU interrupts should be assigned the highest level in the priority sequence. The simplest way to achieve this without performing major surgery on the executive program is to interchange the priorities of the accumulators and the MTU. This scheme requires that the TTY not be used during the actual observation, since its interrupts would interfere with the operation of the accumulators. This is not a severe restriction, since the remote console is available and can be used to control the computer while an observation is in progress.

(2). The tape drive must be made to pause periodically (at least once every 32 kilobytes) to place an inter-record gap on the tape. This restriction is imposed by the IBM tape drives which eventually read the tapes written at the observatory.

(3). The 12-bit accumulator data must be truncated, if necessary, to fit 8 bits, if data output is to keep up with input. Truncation is preferable to reducing the count rate by use of optical attenuation in the photometer, since truncation has less effect on the signal/noise ratio of the observation than does attenuation. (For photon-counting systems, the signal-to-noise of a measurement depends on the square-root of the effective count rate. Attenuation, of course, directly reduces the effective count rate. On the other hand, truncation reduces both the signal and the noise of a measurement by approximately the same factor, leaving their ratio almost unchanged. Thus truncation does not significantly alter the effective count rate.) Also, truncation allows more flexibility for last-minute changes (an occultation will not wait while the observer inserts or removes a filter from his photometer). Of course, some optical attenuation may still be required to protect the photomultiplier if the event being observed involves a bright star and/or a high lunar background.

(4). The specific data structure used is a queue, which resides in the memory of the computer. A queue is a "circular" data structure characterized by simultaneous and independent data input and output. Once the system is started, the accumulators are allowed to run until the queue is filled. Several cycles through the queue are possible before this happens, since the tape drive is removing data from the queue at approximately the same rate as they are arriving from the active accumulator. Alternatively, the accumulators can be shut off by a command from the remote console. Conveniently, it has been found that

the tape drive actually operates at a rate of about 985 bytes/sec; this, plus the fact that the tape drive has been made to pause at the end of each cycle through the queue to place an inter-record gap on the tape (a procedure which takes about 450 milliseconds), ensures that the accumulator will eventually succeed in filling the queue if the program is allowed to run long enough.

3.4 The Data-acquisition Program: Operation

The data-acquisition program is divided into four sections.

(1). A program segment, executed through the TTY, which prepares the system for operation, and then terminates. In this segment the observer specifies the location and length of the data queue in memory. This, in turn, determines the length of the run. The longest possible observing run is currently about 5 minutes in length.

(2). A console segment, which is executed upon command from the remote console. This segment begins the actual observing run. It reads the truncation (0-4 bits) as set by the observer on a console thumbwheel, incorporates it into the program, enables the accumulators, and then terminates.

(3). A counter segment, which accepts, trims, and queues the incoming data. During the first 250 milliseconds of operation, this segment does

not queue photometric data, but rather stores the seconds and 0.1 seconds digits from the UT clock at each interrupt from the frequency-standard. This serves to establish the absolute timing of the record, as long as the observer maintains a fairly accurate idea of the starting time. After this interval, the tape drive is enabled and photometric data is queued. The segment also monitors the conditions responsible for accumulator interrupts, keeping and displaying on the remote console the running logical sum of these conditions. This warns the observer of any abnormalities, in particular, a "Lost Data" condition, which may occur during the run. This segment remains active until the data queue is filled or a "Halt" command is received from the console.

(4). A tape segment, which transfers the queued data to the tape under interrupt control, and places inter-record gaps on the tape after each pass through the data queue. This segment terminates after emptying the queue the final time. The system can then be prepared for another run by executing the program segment, which takes about 30 seconds.

3.5 General Remarks on the Observation of Occultations

The system described here came into operation during December 1976, and the first observation was made on 2 January 1977. Since the direct setting of the observatory UT clock from WWV time signals has become available only recently, all 1977 timings are accurate only to the ability of the observer to start the computer program at a pre-selected

instant while listening to the WWV signal and/or viewing the observatory clock. This accuracy is probably about 0.2 second. The observing program was not given particularly high priority until after 20 October 1977, when a major stellar occultation was successfully recorded.

Evans (1977) has reported that the Texas group has accumulated a list of some 57 different ways in which an occultation observation can fail, including the presence of trees in the line of sight. Although the Illinois list is not yet quite as extensive, it does include a respectable number of entries. The most frequent cause for failure has been the presence of clouds in the critical part of the sky at the critical moment. Other failures have been caused by winter blizzards blocking access to the observatory, inability to open the dome shutters, tape drive failures, pointing the telescope incorrectly to observe a reappearance, and (yes!) the presence of trees in the line of sight. The number of human failures will, hopefully, decrease with experience, but many failures will remain beyond human control. An occultation observer must simply be prepared for disappointments. However, a rather informal review of the 1977 experiences indicates that about 1/3 to 1/2 of all attempted observations were successful, if multiple observations made in quick succession during one night are counted as a single attempt.

IV. The Analysis of Observational Data

4.1 Review of Techniques for Data Analysis

Over the past forty-odd years, two rather different approaches to the problem of analyzing lunar occultation data have evolved. One involves fitting a theoretical model directly to the observational trace, using the standard procedures of regression analysis. The other, restoration analysis, uses the methods of Fourier analysis to extract the strip image of the occulted source directly from the observed diffraction pattern.

Model fitting was first used to analyze occultation data by Whitford (1939). The application of model fitting is, of course, not unique to occultation data. The basic computational methods are well developed and widely used (e.g., Orear, 1958; Draper and Smith, 1966). Briefly, analysis through model fitting requires that the process being modeled be described in terms of a limited number of model parameters. In addition, if the model is to have much interpretive value, these parameters should correspond to physically meaningful characteristics of the modeled process. The fitting procedure prescribes some systematic method for adjusting the values of the model parameters so as to identify that model which "best" resembles the data, as judged by an appropriate fitting criterion, which is often the well-known principle of least-squares. The values of the parameters characterizing this best fit model are then considered to be the best estimates of the "true" values for the parameters afforded by the data.

Unfortunately, analysis of occultation data through model fitting

is a process of considerable numerical complexity. Even the simple (and nonphysical) case of a monochromatic, unresolved, single star observed through a point aperture requires the use of four model parameters: the time of geometric occultation, the lunar background intensity, the time scale of the event (which is determined by the shadow velocity), and the amplitude (which is determined by the undisturbed stellar intensity). If an observational trace is regarded as a record of intensity as a function of time, these four parameters serve to establish the origins and scales of the two co-ordinate axes. The model is intrinsically nonlinear in these parameters, and, consequently, the estimation of the best-fit values must be performed iteratively.

These considerations alone would imply an analysis of rather forbidding complexity. But, whereas unresolved single stars are indeed encountered in nature, monochromatic observations and point apertures are not. Accurate analysis of even point-source occultations must make corrections for aperture and (especially) optical bandpass, since they affect the shape and spacing of the diffraction fringes and, consequently, the apparent time scale of the event. Each correction enters the model as an integration, which has conventionally been replaced in the analysis by an approximating summation.

If the occulted object itself displays some structure (and it is precisely these cases which are of the greatest astrophysical interest), this structure must also be incorporated into the model. For a star with a resolvable disk, the model must allow for both the angular size of the disk as well as any brightness variations across it (i.e., limb-darkening). Such structure enters the model as yet another

integration. For a binary star, the observed trace is the superposition of two single-star events. Consequently, two occultation times and two amplitudes must be included among the fitted parameters. It should be obvious that the analysis of a complex occultation event can become an awesome numerical problem, indeed.

Model fitting techniques require that the source brightness distribution be rather simple. In particular, arbitrary source distributions cannot be modeled. Fortunately, the optical sources commonly occulted by the moon do, in general, exhibit fairly simple brightness distributions. The same cannot be said for radio sources. This drawback to the model fitting method led, in part, to the development of restoration, or deconvolution, analysis some fifteen years ago. At that time, the observation of radio source occultations was an active field of endeavor among certain groups of radio astronomers. The radio-frequency observation of occultations differs from the optical case in at least one important aspect: radio receivers tend to be more monochromatic (in the sense that $\Delta\lambda/\lambda$ is small) than are optical detectors. Accordingly, a monochromatic approximation is not particularly severe in the radio case, and the bandpass integration can be ignored with relative safety.

The monochromatic form of restoration analysis was originally developed by Scheuer (1962). The salient feature of this technique is that it allows the recovery of the true strip brightness distribution of the source through the convolution of the observed fringe pattern with an appropriate restoring function.

By assuming circular source symmetry, Krishnan (1970) was able to

incorporate an optical bandpass correction into the Scheuer theory. He used his modified procedure to analyze the data from an occultation of a single, resolved star, which had previously been analyzed using model fitting techniques, and obtained essentially the same results.

However, successful application of restoration analysis also requires a priori knowledge of the lunar shadow velocity (recall that this is a fitted parameter in model fitting analyses). For radio occultations, this velocity can be calculated fairly accurately, since the event involves a kilometer or more of lunar limb, and corrections for the lunar limb topography on such a scale are now available. But optical occultations involve only a few tens of meters of limb, and corrections on that scale are not yet generally available. This difficulty seems destined to prevent the widespread use of restoration techniques for analyzing optical occultation data. McCants and Nather (1970), for instance, have concluded that they would rather make the assumptions concerning source geometry required by model fitting, than accept the uncertainties associated with shadow velocity calculations. Currently active workers largely appear to be concurring with that judgment.

4.2 Description of the Analysis Procedures Used Here, and an Example

4.2.1 Preliminary Analysis of Observational Data

The analysis procedure adopted for the investigation of stellar occultations in this dissertation typically begins with a preliminary

examination of the observational trace, for which purpose plots of intensity and integrated intensity, as functions of time, are prepared. The integrated intensity plot, as introduced by Bartholdi (Dunham, et al., 1973), permits easy identification of multiple events by smoothing the noise of the observational trace. If I_i represents the intensity (a photocount) recorded during the i th time frame, and $\bar{I}$ represents the mean intensity per time frame averaged over the interval of interest, the integrated intensity for the n th time frame, $\bar{I}_n$, is defined as

$$\bar{I}_n = \sum_{i=1}^{n} (I_i - \bar{I}) .$$

The integrated intensity plot has the overall appearance of a segmented linear function of time, with each slope change corresponding to a level change - i.e., an occultation - in the intensity record. For the disappearance of a single star, the plot assumes the form of an inverted "V." A multiple event produces a plot with multiple cusps, one for each component occultation. The detailed geometry of the plot depends on the occultation times and the relative intensities of the component stars. This information could, in principle, be extracted from the plot. However, it appears to be preferable to use the integrated intensity plot, as well as the intensity plot, simply as diagnostic tools with which to identify approximate timings and intensities for the events, and supply this information as starting values for the parameters of a model fitting program, since detailed analysis is necessary, anyway, if accurate timings, shadow velocities, and source geometries are desired.

4.2.2 Detailed Analysis: Model Fitting

The model fitting procedures employed here are modified versions of programs originally written by S.D. Tremaine. There are two basic procedures: one analyzes occultations involving single stars, the other analyzes binary star events. Each minimizes χ^2 (the weighted sum-of-squares of errors) by simultaneously adjusting the values of the model parameters. For single star events, the fitted parameters are: the time of geometric occultation, the background level, the shadow velocity, the amplitude of the event, and the angular diameter of the star. Corrections are made for telescope aperture, the spectral response of the system, and the effective temperature and limb-darkening law for the star. The shadow velocity, the angular diameter of the star, or both, may optionally be held fixed during the calculation. For binary star events, the fitted parameters are: the occultation time for the primary star, the time separation between the two occultations, the background level, the shadow velocity, the intensity due to the primary star, and the flux ratio of the two stars. Corrections are made for aperture, spectral response, and the angular sizes, effective temperatures, and limb-darkening laws of the two stars. Optionally, the shadow velocity may be held fixed during the calculation.

Unlike the model fitting programs in use elsewhere, which perform the fit in the time domain, these programs fit in the frequency domain. This feature allows some reduction to the numerical complexity of the fitting procedure, since the convolution integrals of the model become simple products in the transform space (the optical bandpass integral remains). Of course, this saving is partially offset by the necessity

of Fourier-transforming the observational trace, but this need be done but once during the fitting process.

This feature of the fitting programs also suggests a means for minimizing the effects of scintillation noise in the data analysis. As Ridgway, et al. (1977) have pointed out, scintillation affects primarily the lower frequencies ($\leq$10 Hz), whereas the information contained in the fringe pattern usually appears at somewhat higher frequencies ($\sim$100 Hz or so). The contaminated frequencies could perhaps be suppressed, or even ignored entirely, without serious effect on the fit. In fact, since the fitted frequencies are evenly spaced out to the Nyquist frequency, which is normally several hundred Hertz, the contaminated frequencies already represent a rather small fraction of the total, and may not much affect the fit, anyway. These facets of the analysis problem remain to be examined systematically.

4.2.3 Example: SAO 162512

As an illustration of these analysis procedures, consider the 29 July 1977 occultation of SAO 162512 = ρ' Sgr. This is a relatively bright, unresolved star which has shown no convincing evidence of duplicity. The intensity and integrated intensity plots for this event are shown as Figure 4. The rather irregular shape of the cusp in the integral plot is probably due to the distinct fringe pattern which the event displays, rather than multiple events, although this conclusion cannot be firmly established on the basis of the integral plot alone. There appear to be no other irregularities in the plot: in particular, no slope changes are apparent away from the principal cusp. The central

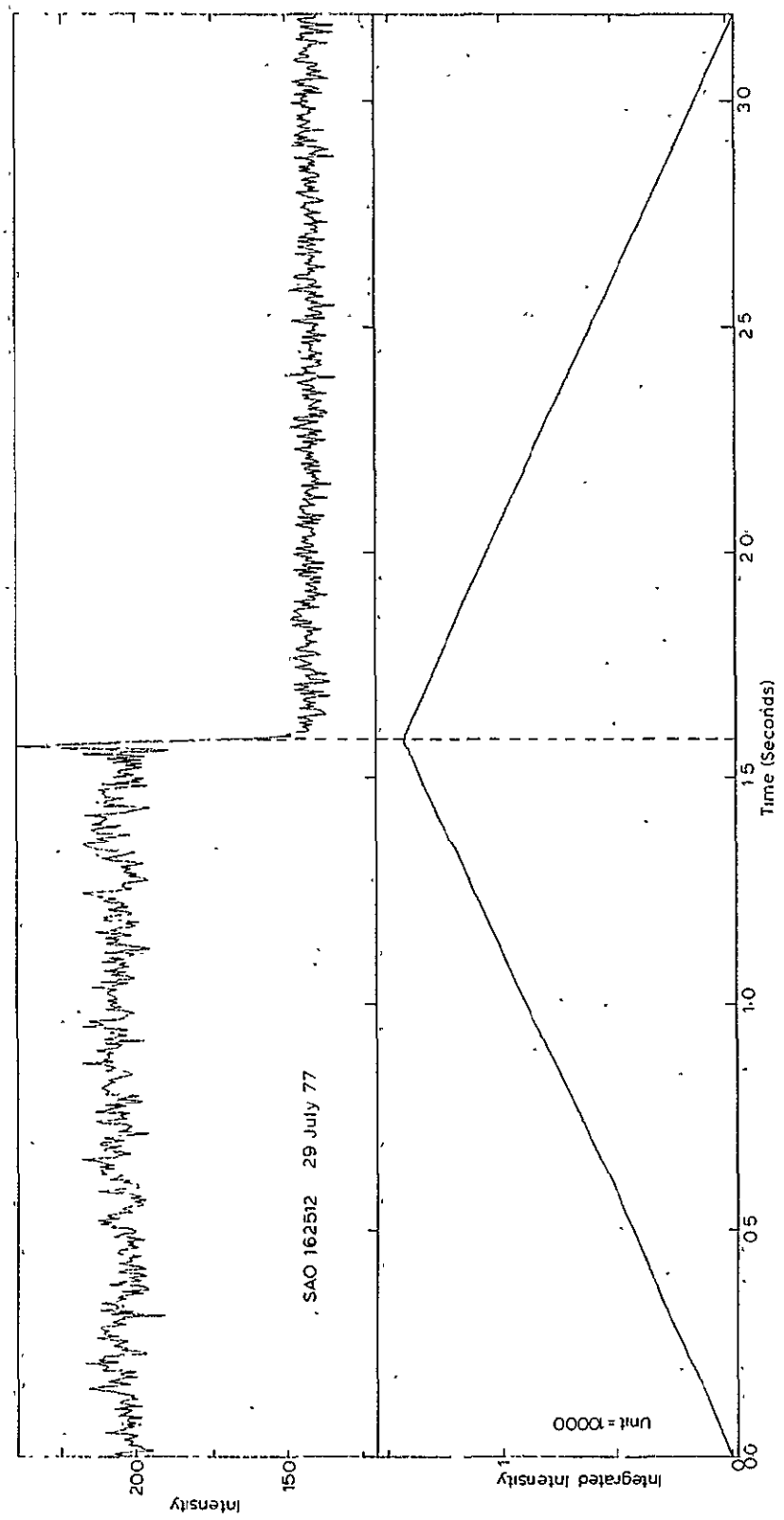

Figure 4 Observational Data, SAO 162512

512 data points, corrected for coincidence losses, were submitted to the single star fitting program. The program was instructed to fit four parameters, keeping the angular diameter of the star (set at 0.33 milliarcsecond) fixed. The best fit is displayed as Figure 5, where the central portions of the observational and model traces are superimposed. The derived shadow velocity has been used to convert the abscissa units to meters, a practice which is becoming standard among occultation observers for the presentation of fitted observations. There appears to be no significant misfit, and the conclusion that the trace is adequately explained as the occultation of a single, unresolved star seems warranted. However, this conclusion must be qualified, as will become apparent later in this discussion.

The derived values for the best-fit model are:

geometric occultation time:	5:13:39.114 ± 0.001	UTC 29 July 1977
background:	141.40 ± 0.96	photocounts/msec
shadow velocity:	0.732 ± 0.01	km/sec
amplitude:	64.54 ± 1.22	photocounts/msec

Since the starting time of the run is uncertain by some tenths of a second, the precision of the time determination is superfluous. However, the derived value for the shadow velocity is of some interest, since it provides information concerning the local slope of the lunar limb at the point of occultation. One defines a compression parameter

$$C = \frac{V_{OBS.}}{V_{PRED}} = \frac{\cos(\varphi - \theta)}{\cos\varphi}$$

where φ is the contact angle and θ the local slope. The contact angle

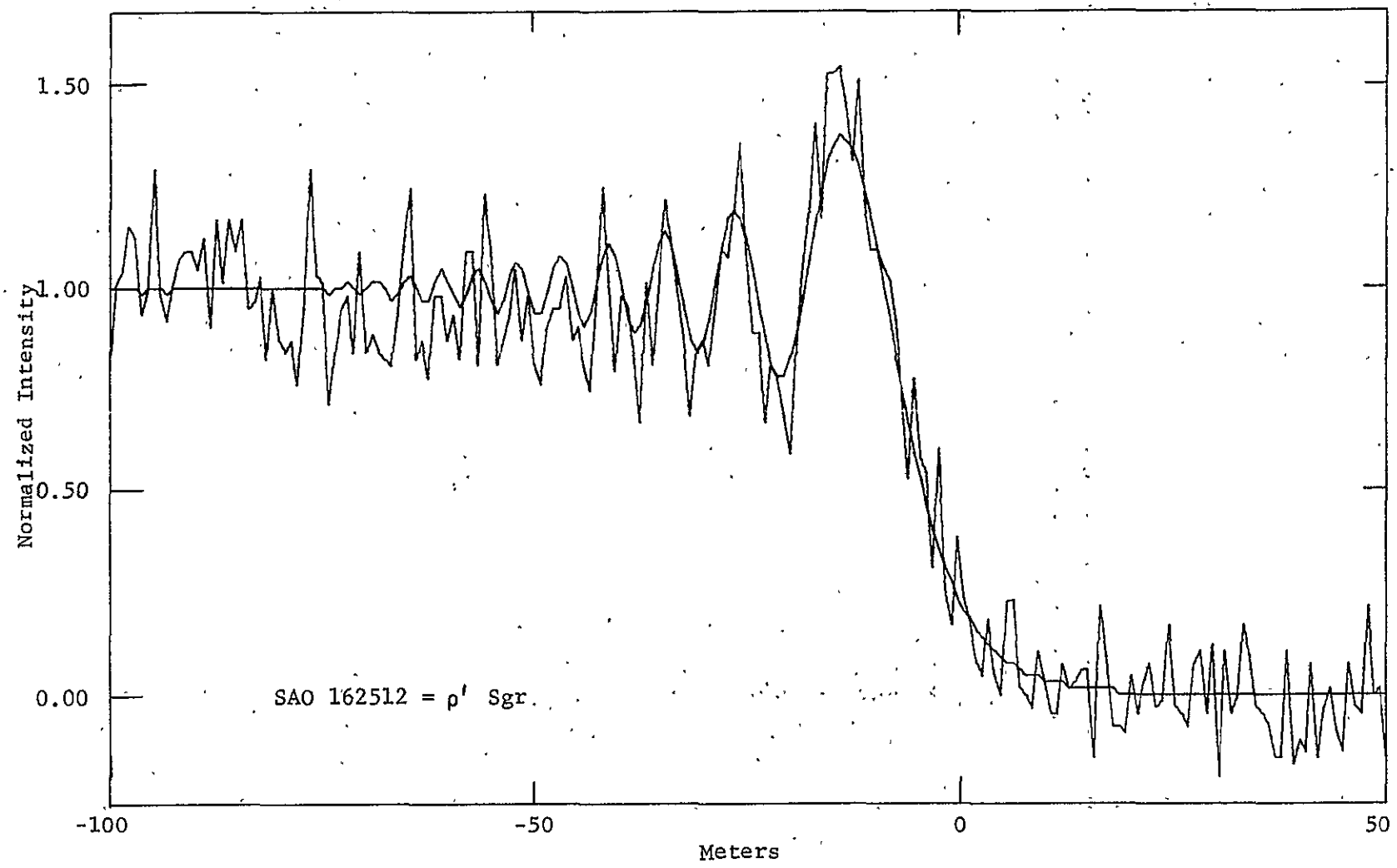

Figure 5 Fitted Data, SAO 162512

is a predicted parameter. In this instance, $V_{PRED.}$ = 0.7328 km/sec and φ = -1.1 degrees. In general, the relation

$$\cos(\varphi - \theta) = \frac{V_{OBS.}}{V_{PRED.}} \cos\varphi$$

may have zero, one, or two real solutions for θ. If there are two solutions, the one which is numerically the smaller is adopted, by convention. The slope is counted positive (regardless of algebraic sign) if C is greater than unity. In this case, C = 0.999, $\cos(\varphi-\theta)$ = 0.999, and θ = 1.8 or -4.0 degrees. The conventional slope is, accordingly, -1.8 degrees.

The conventions concerning limb slopes summarized above constitute what is called the "Texas Sign Convention." This convention is somewhat unsatisfactory, in that the direction of the local normal to the lunar limb at the point of occultation is not unambiguously specified by the position angle of the event and the conventional slope. This direction does not appear to have been given any particular name among occultation observers; I will refer to it as the "aspect" of the occultation. It is defined as follows:

$$\text{aspect} = PA + \theta$$

where the algebraic sign of the slope angle is assumed. In those cases involving two solutions for θ there may remain some ambiguity concerning the aspect, especially if the absolute value of the contact angle is small. In those cases where θ is imaginary, it may be most appropriate to set θ equal to the contact angle in calculating the aspect.

The aspect of an occultation is important because it specifies the direction of resolution for the event. For example, a binary star with components lying perpendicular to the direction of the aspect will not be resolved as it is occulted. In general, only the component of the binary separation in the direction of the aspect is revealed during an occultation, as shown in Figure 6. This component is refered to as the "vector separation" of the two stars.

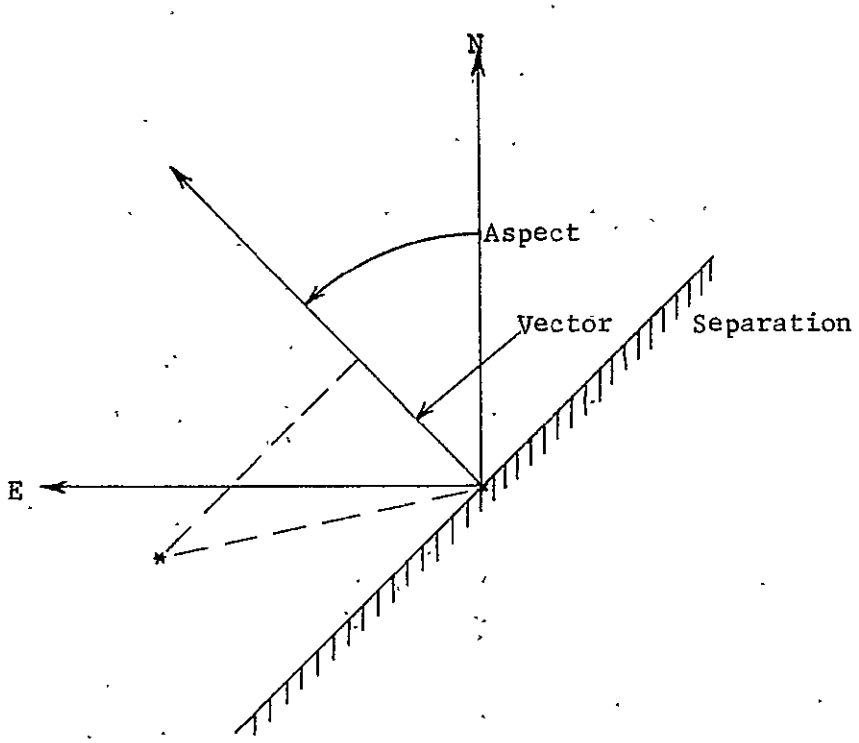

Figure 6 Occultation Geometry: Detail

The aspect of the ρ' Sgr occultation is 78.5 + 1.8 = 80.3 degrees. At this aspect, ρ' Sgr appears to be single, to the resolution limit of an occultation measurement. However, another observation at a different aspect is required before it may be confidently asserted that a star is, in fact, single. An observation of the same event made at another observatory could provide the needed information. Alternatively, since stars tend to be occulted in series of several events, an opportunity to observe a second event at a different aspect may occur for the original observing station.

4.3 Summary of Observations

Tables I, II, and III summarize the occultation observations obtained at Prairie Observatory during the year 1977. The events are arranged in chronological order. The ten columns of Table I contain information derived from the occultation predictions prepared for Prairie Observatory by the United States Naval Observatory. The occulted stars are identified by SAO number in column one. Columns two and three contain the predicted times and dates for the occultations. Times are given in Co-ordinated Universal Time (UTC). The type of phenomenon observed is listed in column four: "D" indicates a disappearance, "R" a reappearance. Columns five six, and seven list the position angles, contact angles, and Watts' angles, as defined in of Figure 2. Columns eight and nine contain the topocentric longitudinal and latitudinal librations of the moon, respectively, and listed in column ten are the predicted values for the lunar shadow velocity.

Table II contains information about the actual observations. Column one again lists SAO numbers. Column two contains the observed times for the occultations. Indicated in column three is the size of the photometer aperture (in arcseconds) used to view each event. Column four lists the spectral filters used. "b" and "y" indicate the standard Strömgren four-color filters generally designated by those symbols. "NB" indicates a filter centered near 6925 Å with a full-width-at-half-maximum (FWHM) of about 510 Å. "FI" indicates a filter centered near 8650 Å with a FWHM of about 300 Å. Column five indicates the number of low-order bits truncated from each time frame for each observation. Column six contains information about the amount of optical attenuation used during each observation. This attenuation is obtained from one or more thicknesses of Wratten No. 96 0.3 neutral density gelatin filter: the number tabulated for each observation is the number of thicknesses used. Information concerning the visual magnitudes and spectral types of the occulted objects, gleaned from a variety of sources, including the USNO predictions and the Bright Star Catalog (Hoffleit, 1964), is listed in columns seven and eight.

The summary is concluded by Table III, in which those events that were fitted are listed. Column one of this table identifies the events by SAO number. In columns two, three, and four the amplitudes, background intensities, and fitted shadow velocities are tabulated (a listing of occultation times would be redundant with column two of Table II, and has not been included). Column five contains the aspects of the events, as defined in the previous section. In column six are listed the algebraic values for the lunar limb slopes, and in column seven, the

"Page missing from available version"

Table I

Summary of Predictions

SAO No	UT Date	Time(p)	Phen	PA	Contact Angle	WA	Long Lib	Lat Lib	Shadow Vel(p)
93849	2Jan77	7:55:55	D	33.4	56.9	45.0	-2.3	4.1	0.4584
(Uranus)	10Feb77	9:32:49	R	238.2	-126.8	219.1	-0.3	-1.0	0.4520
93923	26Feb77	3:12:06	D	59.4	30.0	70.2	-2.8	4.8	0.6337
158492	9Mar77	7:11:08	R	289.9	-177.5	269.6	0.2	-0.7	0.7814
162512	29Jul77	5:13:39	D	78.5	-1.1	86.5	2.1	-5.7	0.7328
163780	23Sep77	5:32:06	D	87.5	-18.2	102.9	3.4	-5.6	0.7902
146043	25Sep77	1:21:29	D	138.8	-70.0	161.3	5.3	-3.6	0.2607
146052	25Sep77	1:31:02	D	107.9	-39.6	130.5	5.3	-3.5	0.5826
146062	25Sep77	2:21:02	D	76.7	-10.2	99.3	5.2	-3.6	0.7120
161376	18Oct77	1:14:32	D	76.8	3.8	78.6	2.6	-5.9	0.8052
163471	20Oct77	2:48:51	D	16.1	54.2	30.0	4.5	-5.8	0.4599
163481	20Oct77	2:53:37	D	21.6	48.7	35.4	4.5	-5.8	0.5215
94173	30Oct77	7:25:44	R	231.6	-149.9	239.4	0.3	6.2	0.5389

Table II

Summary of Observations

SAO No	Time(obs)	Ap	Spect Filter	Trunc	ND	Mag	Spect	Remarks
93849	7:55:54.7	24	NB	3	0?	7.5	G5	1, 5
(Uranus)	9:32:50.5	24	NB	2	1	5.9		
93923	3:12:06.4	16	NB	0	0?	4.2	A2	2, 5
158492	7:11:08.4	16	FI	1	0?	8.7	M5	
162512	5:13:39.1	24?	NB	2?	1	3.94	FOIV	ρ' Sgr
163780	5:32:06.5	12	FI	0	1	7.8	M3	3, 5
146043	1:21:08.8	12	FI	1	1	7.9	M3	
146052	1:30:57.7	12	FI	0	1	9.3	M5	5
146062	2:21:02.9	12	NB	2	1	6.11	gG6	
161376	1:14:31.5	16	y	0	0	5.40	F5p	4
163471	2:48:53.3	16	b	0	0	6.16	B9	
163481	2:53:36.6	24	y	1	2	3.07	comp	β Cap
94173	7:25:42.3	16	FI	0	0	8.5	M4e	5, V Tau

1. Spectroscopic binary, but integrated intensity plot shows no convincing evidence of multiple events. Trace very noisy.
2. Visual binary, 68 Tau. Observation made through heavy clouds: only primary star evident on trace.
3. 0.5 second timing uncertainty.
4. Observed through light haze. Y Sgr (Cepheid)
5. Not fitted: no evidence of multiple events on integrated intensity plot.

Table III

Summary of Reductions

SAO No	Amp	Backgnd	Shadow Vel(c)	Aspect	Slope	Conv Slope	Rmks
158492	35.2	137.5	0.701 ±0.02	266.1 ±3.3	-23.8 ± 3.3	-23.8	
162512	64.5	141.4	0.732 ±0.01	80.3 ±15.5	1.8 ±15.5	-1.8	1
146043	49.1	161.2	0.167 ±0.005	146.1 ±0.4	7.3 ± 0.4	-7.3	2
146062	33.8	160.3	0.784 ±0.03	66.5	no soln.	-	3
161376	86.6	47.7	0.808 ±0.01	80.6	no soln.	-	4
163471	70.4	134.0	0.393 ±0.005	10.3 ±0.4	-5.8 ± 0.4	-5.8	5
163481	180.6	68.9	0.570 ±0.005	26.5 ±0.5	4.9 ± 0.5	4.9	5, 6

1. Second solution for slope: $\theta = -4.0$.
2. A very slow event. An attempt to fit for angular diameter did converge, the best-fit value being 7.229 ± 1.167 milliarcsecond. The solution is probably spurious; the signal/noise for the observation is quite low.
3. $\cos(\varphi - \theta) = 1.084$
4. $\cos(\varphi - \theta) = 1.001$
5. Multiple events.
6. Angular diameter determined.

Indicated uncertainties are formal standard errors.

V. The 20 October 1977 Occultation of β Capricorni

5.1 Background. General Description of the β Capricorni System, As Known Prior to 1975

The extended β Capricorni system contains at least five, probably six, and perhaps as many as eight stars. Three of these stars form the well-known spectroscopic triple system once known as β^2 Capricorni, now known simply as β Capricorni, or SAO 163481. The two principal stars of this system, an evolved giant (β Cap A) and a late B star (β Cap B), form a double-lined spectroscopic pair with a period of some 3.76 years. β Cap B is itself the primary of a single-lined spectroscopic pair with a period of some 8.67 days. The secondary star of this short-period system, β Cap C, although invisible, is presumably a star somewhat similar to the sun. The combined visual magnitude of these three stars is 3.07.

The definitive orbital elements for these two spectroscopic systems were derived by Sanford (1939). At that time plate material from some forty years' observations was available for β Cap A. About four years' worth for the B+C pair, with several months' intensive coverage, was also at hand. Thus several orbital periods of both systems were represented, and the determination of the orbital elements could be made with good precision. Indeed, Batten (1967) still regards the elements for the double-lined system to be among the best available. These orbital elements as derived by Sanford are reproduced as Table IV. Since the long-period system is a double-lined binary, only the angular scale of the orbit and its orientation in space, as represented by the

Table IV

Spectrographic Orbital Elements for β Capricorni

Stars A and (B+C)	
Period (P)	1374.126 ± 2.06 days
Epoch of Periastron Passage (T)	JD 2421521.26 ± 3.25
Argument of Periastron (ω)	119.12 ± 1.29
Eccentricity (ε)	0.417 ± 0.06
a sin(i) β Cap A	395 050 000 km
β Cap (B+C)	360 000 000 km
m sin (i) β Cap A	4.35 $M_\odot$
β Cap (B+C)	4.77 $M_\odot$
Stars (B+C)	
Period (P)	8.6780 days
Epoch of Periastron Passage (T)	JD 2428383.898
Argument of Periastron (ω)	343.24
Eccentricity (ε)	0.36
a sin(i') (β Cap B)	4 226 000 km
m_c sin (i')/(m_β + m_c)	0.040 $M_\odot$

angular semi-major axis of the relative orbit, the orbital inclination, and the position angle of the ascending node, are undetermined by the spectroscopic data. This fact will be exploited subsequently.

In contrast to this excellent knowledge, the spectral classifications of these three stars are surprisingly uncertain. That of β Cap C, G5, is, of course, purely a conjecture based on Sanford's estimate of its mass. The observed spectrum of β Cap B consists of some five lines. Sanford classifies it B8; other opinions range from B7.5 (Ridgway et al., 1977) to A0 (Hoffleit, 1964). However, it is β Cap A which enjoys the truly impressive range of estimates: from F8V (Hoffleit) to gG0 (Sanford) to K0II (Ridgway et al.)

Distant some 205" from these three stars but sharing a common space motion with them is the visual binary ADS 13717, which was once known as β' Capricorni. The brighter star of this pair, SAO 163471, is a B9 star with a visual magnitude of 6.10. Its companion, located some 0.8" away at position angle 84 degrees, has been variously estimated by visual observers to be some four magnitudes fainter than the primary. Judging from the data tabulated in the IDS catalog (Jeffers, et al., 1963), the sense of the apparent motion of the secondary is retrograde, although it has moved through only some 20 degrees in position angle during the past century.

Distant some 227" from SAO 163481 and 398" from SAO 163471, but apparently sharing a common proper motion with them, is SAO 163486. This F8 star has a visual magnitude of about 9.3.

The remaining two stars form the visual binary HJ 2428. These stars, separated by some 6.4", are located some 112" from SAO 163481,

and about the same distance from SAO 163471. The magnitudes of the components are about 13.0 and 13.4. There is no reason other than proximity in the sky for supposing that these two stars are associated with the other six.

The available photometric data on these stars is presented in Table V. The Johnson magnitudes and colors are drawn from the U.S. Naval Observatory Photoelectric Catalog (Blanco et al., 1968) and the Strömgren photometry is that of Stokes (1972). The trigonometric parallax of β Cap is listed as 0.005" ± 0.006" (Jenkins, 1952). These various facts are the salient features of the pre-1975 knowledge of the extended β Cap system.

Table V

Photometric Data

Star	V	B-V	U-B	b-y	m_1	c_1
163471	6.10	-0.02	-0.12	0.000	0.129	0.905
163481	3.07	0.78	0.27	0.518	0.226	0.347

$m_1 = (v-b) - (b-y)$ $\quad c_1 = (u-v) - (v-b)$

5.2. Occultation History and Summary of Observations From Other Stations

It is a curious historical note that β Capricorni was the first star observed photoelectrically while being occulted (Whitford, 1939). Due to its position some 5 degrees north of the ecliptic, β Cap is occulted repeatedly during an interval of two or three years and then not again for some sixteen years. Apparently no photoelectric observations were made of the series which occurred in the late 1950's, but the current series, which began in 1975 and is now ending in the Southern Hemisphere, has been well-observed. In all, some eight different events, concluding with the one on 20 Oct 1977, were visible over North America. Of these, six were visible at the McDonald Observatory of the University of Texas, and five were successfully observed. One of these five events was also observed at the Kitt Peak National Observatory. Prairie Observatory was less fortunate: besides the 20 Oct 1977 occultation, only one other event of the series was visible in a dark sky, and this event was not observed. Of course, other stations may have observed some of these events but have not yet published their results. Table VI summarizes the entire body of occultation data concerning β Cap currently available. For completeness, some of the results of the analysis of the 20 Oct 77 event, as observed at Prairie Observatory, have been included in this table prior to their detailed discussion. Also included in Table VI are binary parameters for the system as derived from a speckle interferometric observation, which will be used at a later point in this analysis.

Table VI
High-resolution Observations of β Capricorni

Obs	UT Date	Orbital Phase	Separation (")	Aspect	Slope	Mag Diff A and (B+C)	Ang Diameter β Cap A (UD) Milliarcsec	Wt	Ref and Note
MO	7Dec75	0.4515	0.0255 ± 0.0010	60.3	N.D.	$\Delta y = 1.8 \pm 0.5$ $\Delta b = 1.1 \pm 0.5$	N.D.	1	1
MO	21Apr76	0.5508	0.022 ± 0.002	90.8	N.R.	$\Delta y = 2.2 \pm 0.4$	N.D.	1	2
KP	21Apr76	0.5508	0.0977 ± 0.0013	98.4	4.3 ± 0.0	$\Delta m = 4.4 \pm 0.2$	3.05 ± 0.12	0	3
MP	26May76	0.5763	0.047 ± 0.005	49 ±6				2	4
MO	26Nov76	0.7099	0.0151 ± 0.0002	293.4	N.D.	$\Delta m_1 = 0.0 \pm 0.1$ $\Delta m_2 = 2.6 \pm 0.4$	N.R.	2	5
MO	15Mar77	0.7895							6
MO	20Oct77	0.9486	0.0068 ± 0.0001	24.0	-2.7 ± 0.4	N.R.	N.R.	3	7
PO	20Oct77	0.9486	0.0086 ± 0.0003	26.5	4.9 ± 0.5	$\Delta y = 1.87 \pm 0.14$	3.13 ± 0.39	2	

MO = McDonald Observatory
MP = Mount Palomar Observatory
KP = Kitt Peak National Observatory
PO = Prairie Observatory

N.D. = not determined
N.R. = not reported

1. Africano et al., 1976. Observed through clouds.
2. Africano and Montemayor, 1977.
3. Ridgway et al., 1977. Observed at 1.67 μ. The binary separation and magnitude difference are almost certainly spurious.
4. Blazit et al.,1977. Speckle interferometric measurement.
5. Africano et al., 1977. m_1 : center=4230 Å, FWHM=400 Å
   m_2 : center=7200 Å, FWHM=2000 Å
6. Apparently observed, but not yet published.
7. Fekel, 1978. Private communication.

5.3 Observation of the 20 October 1977 Events

At the time of the occultations, the first quarter (56% illuminated) moon was 25 degrees above the horizon at Prairie Observatory. The sky transparency was good, although it has been completely overcast shortly before. The seeing was rather exceptional for Prairie Observatory (~2"), although some scintillation remained evident.

The occultations were scheduled to occur in rapid succession, beginning with SAO 163471. SAO 163486 was occulted some two minutes later. Finally, some 4½ minutes after the SAO 163471 event, SAO 163481 was occulted. This order of events, namely, the major occultation last, had considerable influence on the final decisions concerning the observational procedure. No attempt was made to observe the SAO 163486 occultation. Also, it was found necessary to attenuate the light of SAO 163481 with a neutral density filter, whereas SAO 163471 could be observed without attenuation. It was felt that it would be unwise, under the somewhat stressful circumstances of the observation, to observe the SAO 163471 occultation and then attempt to disassemble the photometer to insert the attenuation needed for the second event, a process which would normally take at least two or three minutes. To observe SAO 163471 with the attenuation in place would be to needlessly throw away light, and degrade the signal-to-noise ratio. Accordingly, it was decided to observe the events using two spectral filters occupying different slots in the multi-position filter slide of the photometer; the Strömgren "b" filter was selected for the first occultation, and the Strömgren "y" filter, with the necessary

attenuation, was used for the second. Since the telescope drive was behaving somewhat erratically, the second occultation was viewed through a comparatively large (24") diaphragm, although the SAO 163471 occultation was viewed through a smaller (16") aperture (the importance of the observation and the starlight/background ratio dictating the degree of risk which was felt to be acceptable). A one minute data run was recorded for each star. Mr. William Tetley ably assisted in the observations.

5.4 Data Analysis

5.4.1 SAO 163471 System

The integrated intensity plot for the SAO 163471 occultation is shown in Figure 7. Two slope discontinuities are present, separated by about 1.1 second. Apparently this is the first photoelectric record of an occultation of this binary star which clearly includes two events. Previous observations obtained at McDonald Observatory have only recorded the primary event, due to the limited storage available in the circulating buffer of that observing system.

The two events were fitted separately, using the single star fitting program for each. This procedure is advisable for widely separated events, not only because fitting a long data set is time-consuming, but also (and more importantly) because the lunar background intensity, which the fitting program assumes to remain constant, can change appreciably between widely-separated events. Failure to allow for this could introduce a sizeable systematic error

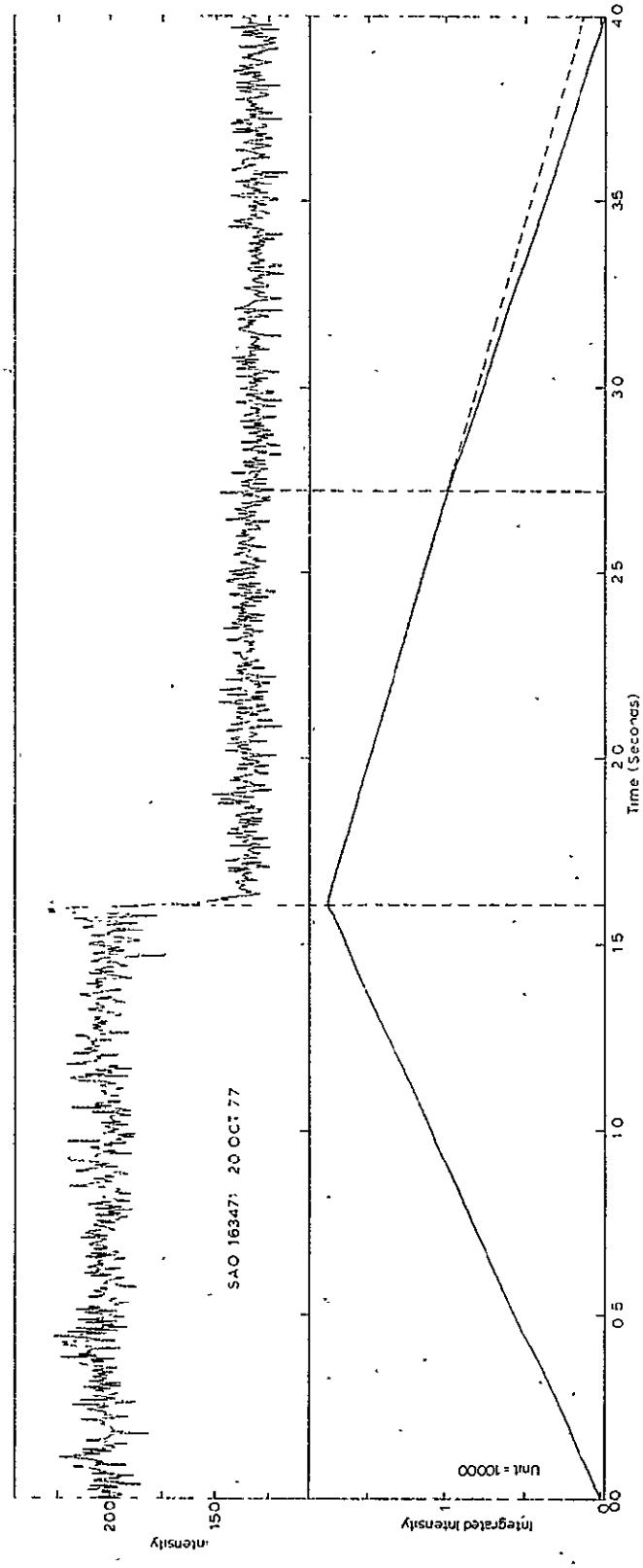

Figure 7 Observational Data, SAO 163471

into the estimate of the amplitude of a secondary occultation involving a faint star. By fitting the events separately, and locally, this possibility is minimized.

The results of these calculations are summarized as Table VII. The vector separation was calculated using the lunar limb distance furnished by the USNO prediction for the event (372038 km) to convert the derived shadow velocity into an angular rate.

5.4.2 SAO 163481 System

The analysis of the SAO 163481 event is somewhat more complex, as it involves a binary system with a resolved component. It would certainly be possible to incorporate the angular diameter of the resolved star directly into the binary star fitting program as a fitted parameter, but this would result in a seven-parameter model, which could be badly behaved, as well as time-consuming to compute. As an alternative to this, an iterative scheme was devised which used the binary star and the single star programs alternately. The binary parameters were first calculated, assuming a 3.1 milliarcsecond disk for the primary (the value indicated by the Kitt Peak observation of Ridgway et al., 1977). Using these results, the diffraction pattern due to the secondary star was calculated and removed from the observational trace. The resulting trace was then fitted as a single resolved star. The diameter for the primary so determined was then supplied to the binary-star program, and the cycle repeated. In practice, the second iteration resulted in no significant changes in the binary parameters, and the process was halted.

Table VII

Summary of Results, SAO 163471

	Primary	Secondary
Amplitude	66.51 ± 1.25	3.89 ± 0.77
Shadow Velocity	0.393 ± 0.005	0.393 (assumed)
Δb	3.08 ± 0.22	
ΔT (msec)	1121.4 ± 8.0	
Slope	-5.8 ± 0.4	
Aspect	10.3 ± 0.4	
Vector Sep.(")	0.244 ± 0.050	

Indicated uncertainties are formal standard errors.

This procedure demonstrated directly that changes on the order of a few tenths of a milliarcsecond in the assumed angular diameter of the primary have no appreciable effects on the values of the derived binary parameters, and this, in turn, argues that the synthetic trace calculated for the primary star alone probably contains no significant artifacts due to the secondary star. This trace was subjected to further analysis. Fits were performed for the two "standard" limb-darkening options, the uniformly-illuminated disk and the fully-darkened disk in which the emergent intensity varies as the cosine of the angle between the observer's line of sight and the normal to the stellar photosphere, at each surface point. The uniqueness of the angular diameter fits was also checked by running the program with initial values for this parameter significantly larger as well as smaller than the best-fit value. The fit always converged to the same final value, well within the standard error of the fit, unless some really bizarre initial value was used. The results of these calculations are summarized in Table VIII. The vector separation was calculated using the predicted limb distance of 372109 km. The observational data for this event are displayed as Figure 8, and Figure 9 shows the model fit superimposed on the central portion of the observational light curve.

5.5 Intepretation and Discussion

5.5.1 Individual Magnitudes and Colors

The occultation data, in conjunction with the photometric data of

Table VIII

Summary of Results, SAO 163481

Primary Time	2:53:36.598 ± 0.0003
Background	68.92 ± 1.02
Shadow Velocity	0.571 ± 0.002
Primary Amplitude	153.18 ± 3.05
Time Separation (msec)	27.02 ± 0.96
Amplitude Ratio	0.179 ± 0.023
Δy	1.87 ± 0.14
Slope	5.0 ± 0.2
Aspect	26.6 ± 0.2
Vector sep. (")	0.00855 ± 0.00031
(limb distance = 376109 km)	

Limb-Darkening Law	Ang Diameter Milliarcsec	Slope
Uniform Disk	3.13 ± 0.39	4.7 ± 1.0
Fully-Darkened Disk	3.54 ± 0.46	4.8 ± 1.0

Indicated uncertainties are formal standard errors.

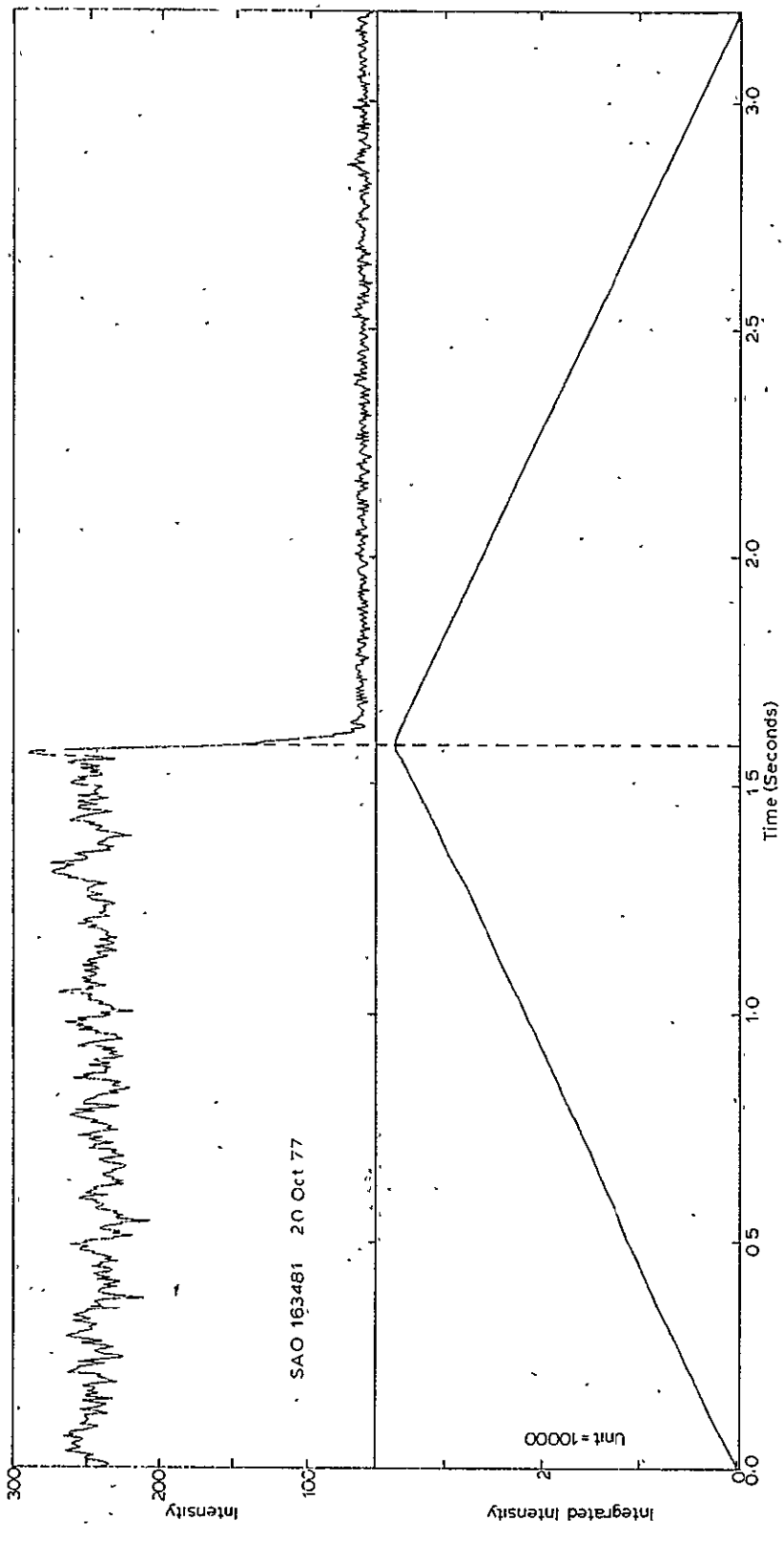

Figure 8 Observational Data, SAO 163481

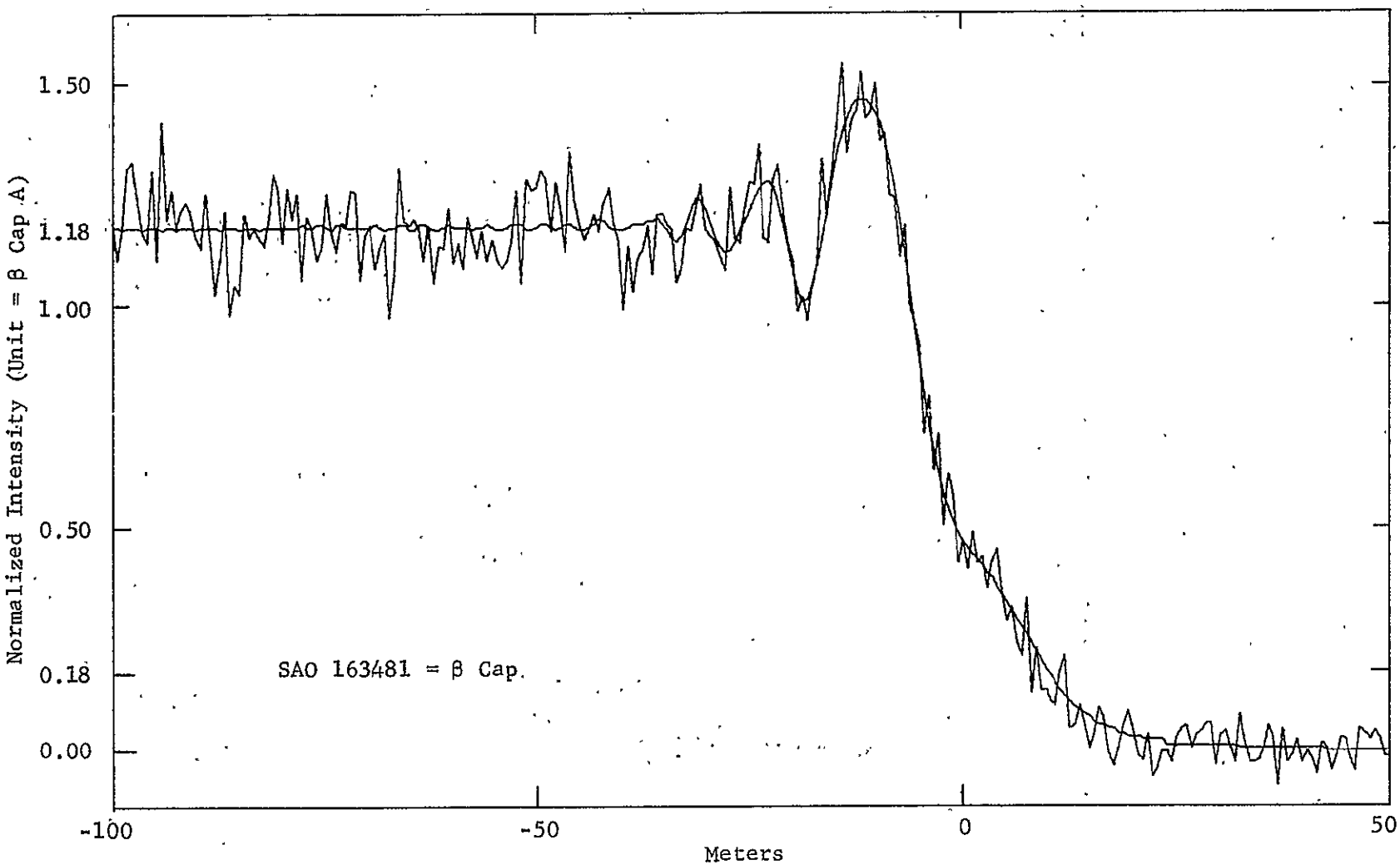

Figure 9 Fitted Data, SAO 163481

Table V, permit the calculation of individual magnitudes and colors for the component stars of these two systems, if it is assumed that Johnson visual magnitudes are equivalent to Strömgren "y" magnitudes.

For SAO 163481, if $\Delta y = 1.87$ and $\Delta b = 1.1$ (from the 7Dec75 Texas observation),

$y_A = 3.25$ $\quad b_A - y_A = 0.68$
$y_{B+C} = 5.12$ $\quad b_{B+C} - y_{B+C} = -0.09.$

For SAO 163471, the b-y color for the primary must also be assumed: the standard list of Crawford and Barnes (1970) indicates that a color of -0.02 is reasonable for such a star. Then

$y_A = 6.18$ $\quad b_A - y_A = -0.02$ (assumed)
$y_B = 8.97$ $\quad b_B - y_B = 0.27$

Since the primary star almost certainly must belong to luminosity class V, the implied spectral type for the secondary is about F4V, from its color.

5.5.2 Spectroscopic Parallax

By adopting the values tabulated by Allen (1973) for the absolute magnitudes of the main sequence, distances to these various stars may be inferred:

for SAO 163481, 150 pc, 125 pc, or 110 pc, if β Cap B is a B6V, B7V, or B8V star, repectively;

for SAO 163471, 150 pc or 125 pc, if the star is a B9V or A0V star, respectively;

for SAO 163486, 115 pc, if the star is a 9.3 magnitude F8 star.

There is no reason to suppose that the stars are significantly dimmed by interstellar extinction: they are comparatively near by, their galactic latitude is some 26 degrees, and they do not appear to be reddened.

There can be little doubt that the SAO 163481 and the SAO 163471 systems are physically associated, and at roughly the same distance from the sun. Not only do they share common proper motion, but the radial velocities of SAO 163471 and the center-of-mass of SAO 163481 agree to within 2 km/sec (Abt and Biggs, 1972; Sanford, 1939), and are comparable to the the implied transverse velocities, assuming a distance of 130 pc or so. An angular separation of 205" at this distance corresponds to a linear separation of 0.13 pc in the plane of the sky; the radial separation cannot be much different from this. Although the evidence is less conclusive for SAO 163486, it seems reasonable to suppose that it is also physically associated with SAO 163471 and SAO 163481, since it appears to share a common proper motion with these systems, and is apparently at about the same cistance.

The composite b-y color for SAO 163471 suggests that the spectral classification of the primary, B9V, is probably quite accurate. Also,

the derived b-y color for β Cap B suggests a somewhat earlier spectral class than B7.5 to A0. It is possible, of course, that this star is indeed over-luminous; the palpable fact that β Cap A, which is only some 15% more massive than β Cap B, is an evolved star argues that β Cap B itself may no longer be on the main sequence. These arguments suggest that the larger distance of 140-150 pc may be appropriate as the distance to the extended system.

On the other hand, the spectral classification and visual magnitude of SAO 163486, if accurate, and the spectral classification of β Cap B both suggest a distance in the range 110-120 pc. There being no preponderance of evidence, it is perhaps best to adopt a distance of 130 pc, midway between the two, bearing in mind that this may be uncertain by some 20 pc or so.

5.5.3 Effective Temperature and Spectral Class of β Cap A

This distance implies a linear radius of some 51 $R_{\odot}$ for β Cap A, and an absolute visual magnitude of -2.3, which clearly places this star in luminosity class II. This established, the effective temperature and spectral class of this star may be determined. The right-hand side of the relation

$$\log T_e + 0.1\,B.C. = 4.2207 - 0.1\,V_o - 0.5 \log \phi'$$

(Barnes and Evans, 1976), where Te is the effective temperature, B.C. the bolometric correction, Vo the unreddened apparent visual magnitude, and ϕ' the angular diameter of the star in milliarcseconds, may be

calculated directly. Since a star such as β Cap A is likely to be rather heavily limb-darkened in the visual (Ridgway et al., 1977), the appropriate value to use for the angular diameter is that derived using the fully-darkened disk option. Thus

$$\log T_e + 0.1\,B.C. = 3.62$$

Interpolating among the effective temperatures and bolometric corrections tabulated by Allen (1973), it is found that a bolometric correction corresponding to a spectral class of about G8II, and the effective temperature for such a star, 4600 K, satisfy this relation. Alternatively, one could assume a bolometric correction, and calculate an effective temperature for this star, which would be uncertain by 300 K or so, as determined by the uncertainty in the angular diameter measurement. Supposing that the identification of β Cap A as a G8II star with an effective temperature of 4600 K is correct, a bolometric magnitude of about -2.74 is indicated, or a luminosity of some 990 suns.

5.5.4 Orbital Analysis

5.5.4.1 The General (Three-parameter) Analysis

The elucidation of the physical characteristics of the β Cap system may be approached from another direction. It is possible, using the data of Table VI and the Sanford spectrographic elements, to determine the angular scale and spatial orientation of the relative orbit of β Cap A and β Cap (B+C).

From the spectroscopic elements, one knows the shape of the true relative orbit (eccentricity), the position of the secondary star (β Cap (B+C)) along the relative orbit at any time (period and epoch), and location of the line of nodes (the line of intersection between the orbital plane and the plane of the sky) relative to the true orbit (argument of the periastron). The spectrographic elements do not distinguish between direct and retrograde motion; these two possibilities correspond geometrically to two possible orbits having reflection symmetry about the semi-major axis.

Consider a right-handed Cartesian co-ordinate system, located in the plane of the true orbit, centered on the primary star, with the X-axis directed along the line of nodes. For the direct orbit, the ascending node is in the direction of the positive X-axis; for the retrograde orbit, the descending node is in this direction. Let the unit for both co-ordinates be the semi-major axis of the true relative orbit. At any instant - that of an occultation, for instance - the Cartesian co-ordinates of the secondary star can be calculated: if these co-ordinates in the direct orbit are (x,y), those in the retrograde orbit are (-x,y). This geometry is illustrated in Figure 10, which represents the retrograde orbit. The five dated points locate the secondary star at the times of the observations listed in Table VI.

By means of two rotations and a rescaling, co-ordinates in this system can be transformed into those of an angular system centered on the primary star and lying in the plane of the sky. The first rotation, about the line of nodes, inclines the orbit with respect to the plane of the sky. If this inclination is i, the transformation equations are

$$X_I = X \quad , \quad y_I = y \cos i$$

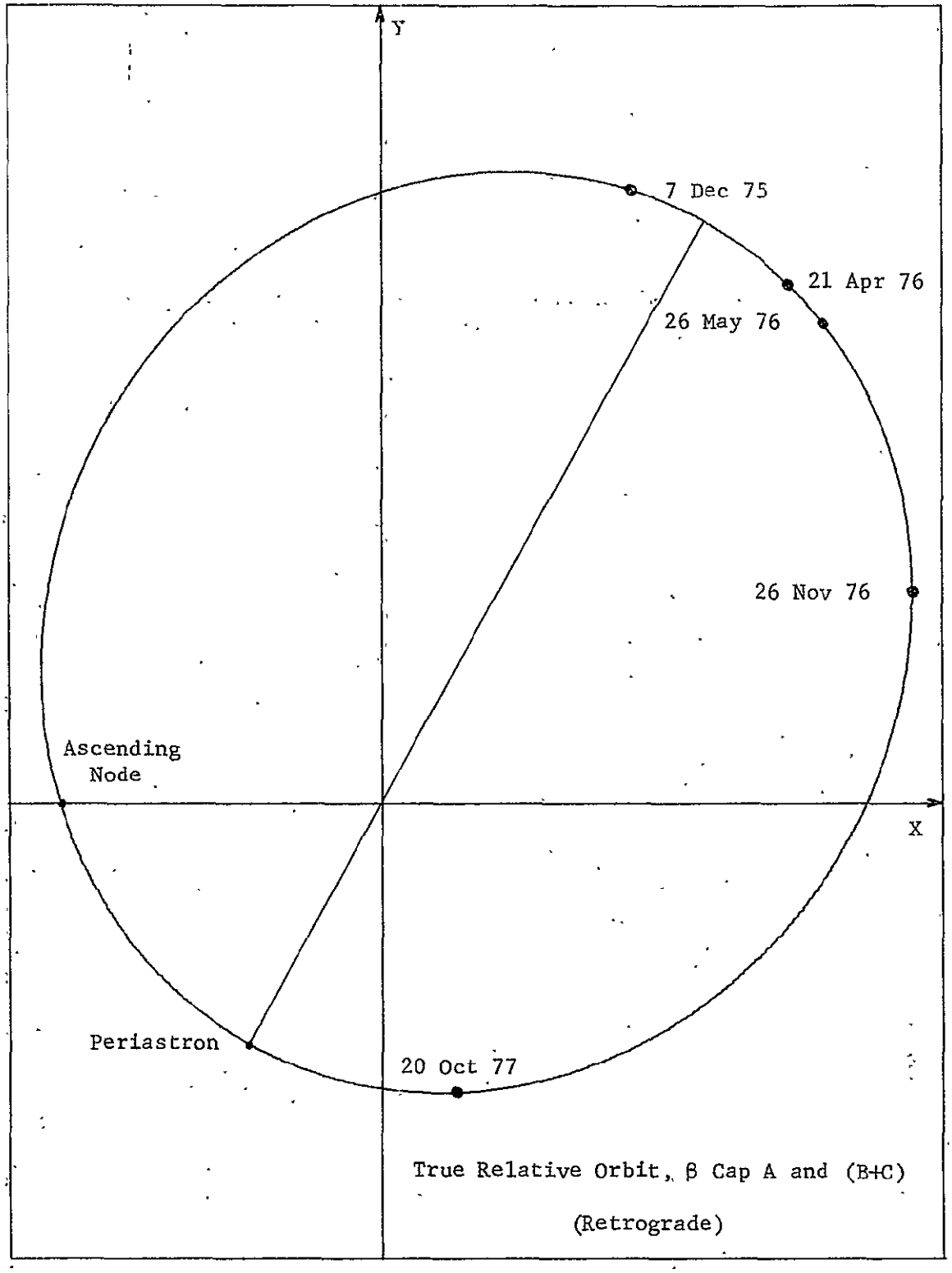
Y
7 Dec 75
21 Apr 76
26 May 76
26 Nov 76
Ascending
Node
X
Periastron
20 Oct 77
True Relative Orbit, β Cap A and (B+C)
(Retrograde)

Figure 10

where (x,y) are the original co-ordinates of the secondary star. The second rotation, about the line of sight, corrects the orientation of the projected orbit in the plane of the sky. The transformation equations may be written as

$$X_{II} = X_I \cdot \cos\Omega' + y_I \sin\Omega' , \quad y_{II} = -X_I \sin\Omega' + y_I \cos\Omega' .$$

The angle Ω' is related to the position angle of the ascending node, Ω; for the direct orbit, $\Omega' = 270 - \Omega$, whereas for the retrograde orbit, $\Omega' = 90 - \Omega$. In the (x_{II},y_{II}) system, the positive x_{II} axis is directed westward in the sky. The final transformation converts the units to angular measure: if the scaling factor be represented as a", the transformation is represented simply as

$$X_{III} = a'' X_{II} , \quad y_{III} = a'' y_{II} .$$

Each occultation observation of a binary star provides a relation between x_{III} and y_{III} of the form

$$y_{III} = A_1 X_{III} + A_2 .$$

This may be demonstrated by refering to the geometry of Figure 6. It is apparent that an occultation does not uniquely determine the relative positions of the two stars. Rather, the position of the secondary star, relative that of the primary, may be anywhere along a line perpendicular to the direction of the aspect, which has the vector separation as its closest approach to the position of the primary. The parameters A_1 and

A_2 are the slope and intercept, respectively, of this line-of-possible-position. Combining all these relations and expressing the final form in terms of x, y, A_1 , A_2 , and the undetermined parameters i, Ω', and a" produces the equation

$$a''(A_1 x \cos\Omega' + A_1 y \cos i \sin\Omega' + x \sin\Omega' - y \cos i \cos\Omega') + A_2 = 0$$

A speckle interferometric observation, which does determine the relative positions of the two stars, except for a 180 degree ambiguity in position angle, may be considered equivalent to two occultation observations with perpendicular lines-of-possible-position which intersect at the location of the secondary, if the position angle ambiguity can somehow be resolved. In this particular case the resolution is simple, since the speckle observation and one of the occultations happened to occur almost at the same time. Only one of the two possible speckle positions lies anywhere near the line-of-possible-position determined by the occultation, and is therefore identified as the correct one.

The model represented by the above equation was optimized in terms of the parameters i, Ω', and a" using the non-linear least-squares fitting routine of the SAS76 statistical package, which is available at the University of Illinois computing center. Excluding the Kitt Peak observation, which was rejected as being clearly inconsistent, the observations of Table VI were assigned weights, ranging from one to three, based on a personal estimation of their probable relative accuracies. These weights are indicated in Table VI. Each weight was

determined by the number of channels used for the observation, the observing conditions, and the quality of the trace as indicated by the formal errors derived in its analysis. The two equivalents for the speckle observation were each assigned unit weight. Preliminary inspection demonstrated conclusively that it is impossible to orient a direct orbit in any way so as to even remotely satisfy all the observations. Thus, it was necessary to fit only for the retrograde orbit. The best-fit parameter values for this orbit, and their formal standard errors, are

(Solution A)

$i = 67.8 \pm 13.7$
$\Omega = 183.4 \pm 9.6$
$a'' = 0.048 \pm 0.013$

The apparent orbit, as determined by these calculations, is shown in Figure 11. The heavy, dated dots represent the calculated positions for the secondary, and the short line segments represent the locii of possible position as derived from the occultation data. The box locates the region of possible position for the secondary as indicated by the speckle interferometric observation and its standard errors.

5.5.4.2 Two-parameter Analysis (Distance Assumed)

It is also possible to assume a distance to the system, thereby fixing the angular scale of the apparent orbit, and fit for its orientation alone. Formally, this amounts to replacing the parameter a"

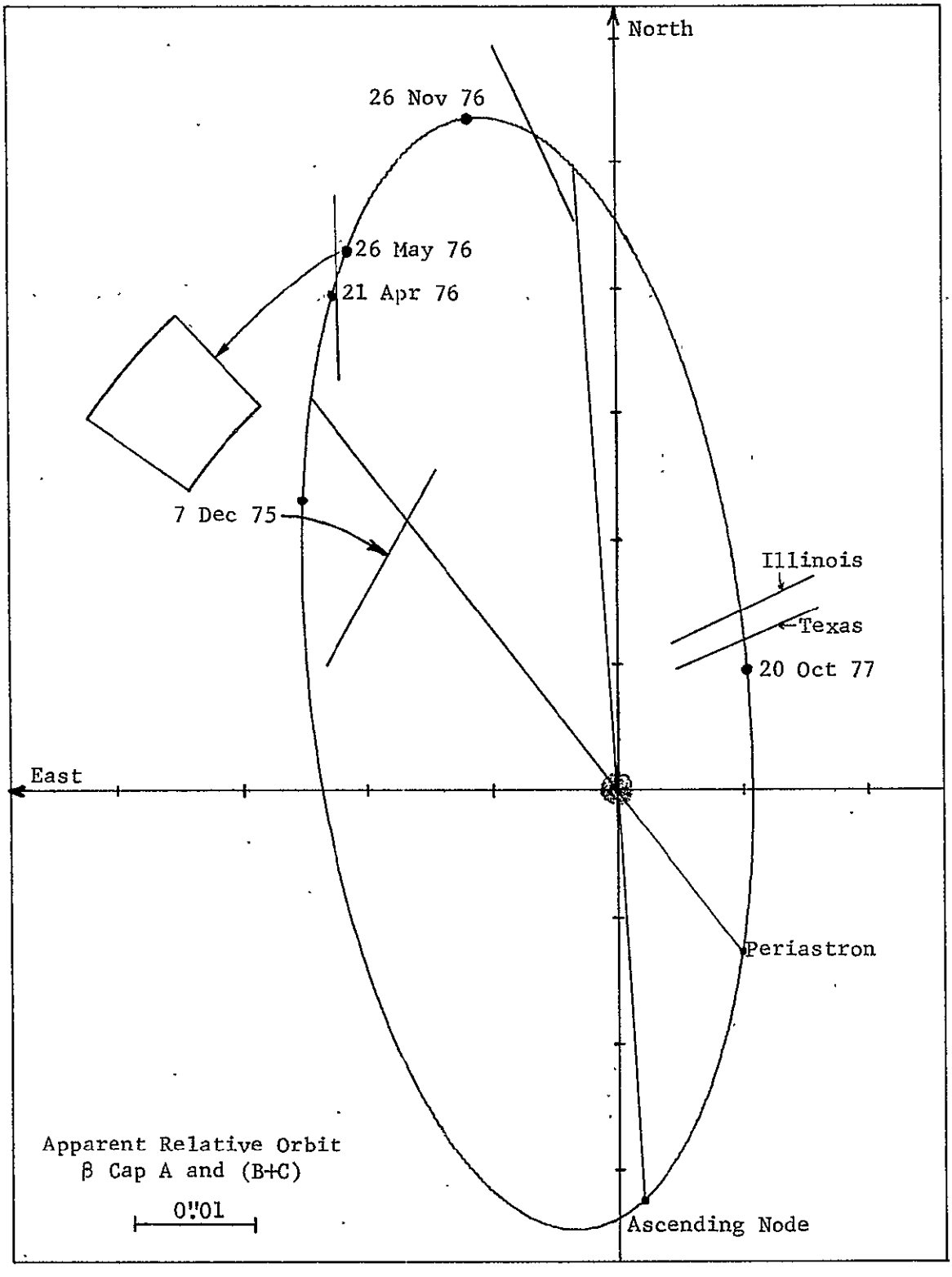
North
26 Nov 76
26 May 76
21 Apr 76
7 Dec 75
Illinois
Texas
20 Oct 77
East
Periastron
Ascending Node
Apparent Relative Orbit
β Cap A and (B+C)
0".01

Figure 11

with c/sin(i), where c is a constant determined by the selected distance. For a distance of 130 pc, c = 0.0391, and the best-fit parameters are:

(Solution B)

$i = 63.6 \pm 3.9$
$\Omega = 181.4 \pm 5.7$
$a'' = 0.044 \pm 0.002$

5.5.4.3 Results

Table IX presents values with standard errors for various physical parameters characterizing the stars of the β Cap system, as inferred from these two orbital solutions and the data tabulated previously.

For Solution A, the inferred magnitudes are characteristic of a G8II and a B8V star. Assuming a mass of 1.22 $M_\odot$ for β Cap C, a mass of 4.79 $M_\odot$ for β Cap B is appropriate for a B7V or a B8V star, while β Cap C would be a F6V star.

For Solution B, masses of 5.28 $M_\odot$ and 1.35 $M_\odot$ for β Cap B and β Cap C, respectively, are appropriate for B6V or B7V and F5V stars.

5.5.5 Comments on Evolutionary Calculations

Evolutionary tracks published by Becker et al. (1977) indicate that a 5.5 to 6.0 $M_\odot$ star could indeed have an effective temperature of about 4600 K and a luminosity of 900 $L_\odot$ or so during the comparatively long-lived portion of its life immediately following core helium ignition, if the chemical composition of the star is roughly solar.

Table IX

Physical Parameters, SAO 163481

Parameter	Solution A	Solution B
Mass (β Cap A)	5.48 ± 1.60 $M_\odot$	6.05 ± 0.60 $M_\odot$
Mass (β Cap (B+C))	6.01 ± 1.76 $M_\odot$	6.63 ± 0.66 $M_\odot$
Mass (β Cap C sin(i'))	1.13 ± 0.22 $M_\odot$	1.21 ± 0.08 $M_\odot$
a_{REL} (β Cap A and (B+C))	5.45 ± 0.53 A.U.	5.64 ± 0.26 A.U.
Distance	114 ± 33 pc	130 pc (assumed)
Radius (β Cap A)	43 ± 14 $R_\odot$	51 ± 7 $R_\odot$
Mv (β Cap A)	-2.0 ± 0.6	-2.3
Mv (β Cap (B+C))	-0.2 ± 0.6	-0.5
Luminosity	770 ± 450 $L_\odot$	990 $L_\odot$

i' = inclination of short-period orbit. If i' = i,

Mass (β Cap B)	4.79 ± 1.52 $M_\odot$	5.28 ± 0.56 $M_\odot$
Mass (β Cap C)	1.22 ± 0.24 $M_\odot$	1.35 ± 0.10 $M_\odot$

However, the exact luminosity depends critically on the chemical mix assumed. Without compositional data for β Cap A, it is difficult to infer much from a comparison of observational data and evolutionary calculations.

5.5.6 Comments on Further Needed Observations

To improve the accuracy of the orbital determination for the SAO 163481 system, it would appear to be desirable to obtain a current measurement of the orbital phase of β Cap A and (B+C), in order to more securely tie the spectroscopic elements to the modern high-resolution observations. These observations themselves may be further augmented if other observers still have occultation observations to report, or if additional speckle interferometric observations are made, as would seem warranted.

It is unfortunate that more occultations of SAO 163471 have not been successfully observed; if observational colors and magnitudes for the individual stars of this system were available, it would be possible to fix the spectroscopic distance to that system, and thus to β Cap itself, much more securely. One can only hope that additional occultaion observations of this system yet remain unreported. The MK spectral classification for the primary could perhaps be examined more closely spectrographically.

It is apparent that more attention ought to be paid to SAO 163486. It appears to be an isolated, main-sequence star; an occultation observation (Africano et al., 1977) revealed no companion brighter than 12th magnitude. If (as seems quite likely) this star is physically

associated with the extended β Cap system, it may offer the best opportunity for establishing an accurate spectroscopic parallax for the system. Radial velocity measurements and a closer examination of its proper motion are needed to confirm its relationship to the other stars. Radial velocity measurements scattered over a period of a few years would also help determine whether or not the star is, indeed, single. An accurate MK spectral classification and precise photometry are, of course, essential for obtaining a reliable spectroscopic distance to this star.

The binary HJ 2428 should also be investigated more thoroughly. If these two stars are members of the group, they must both be late K stars. Obviously, the useful work on the stars of the extended β Capricorni system is far from completed.

VI. The 10 February 1977 Occultation of Uranus

6.1 Background

Although the planet Uranus has been regularly observed for almost two centuries, many of its physical characteristics remain poorly known. The planet, located some 19 A.U. from the sun, appears both small (angular diameter ~4") and faint (visual magnitude ~6). Ground-based telescopes cannot clearly image Uranus, because atmospheric seeing effects distort and blur its small disk. For these reasons, it is extremely difficult to accurately measure the the angular size of the planet, or to study the detailed appearance of its disk.

The photographs obtained by Danielson et al. (1972), using the balloon-borne Stratoscope II telescope, have provided the best modern observational information about the size and appearance of Uranus in the visual region of the spectrum (3800 Å to 5800 Å). These photographs show a strongly limb-darkened disk which is otherwise featureless, having and equatorial radius of 25900 ± 300 km and an ellipticity of 0.01 ± 0.01.

The infrared spectrum of the planet shows deep absorption bands due to methane in its atmosphere. Sinton (1972) and Smith (1977), observing in the 8870 Å band, and Franz and Price (1977), observing in the 7300 Å band, have found the disk to be limb-brightened in and around these spectral features. These observers have also found brightness variations across the disk which are best explained as a general brightening over the polar region of the planet. Sinton measures the equatorial radius to be 27300 ± 1300 km, while Smith measures it as

27900 ± 500 km.

When observing Uranus, it is its atmosphere, or, more properly, those layers of its atmosphere which scatter the greater share of the incident radiation, being observed. Presumably, the strongly absorbed infrared wavelengths are scattered from higher layers than are the more weakly absorbed visual wavelengths. However, this alone probably cannot account for the rather sharp disagreements among the size measurements. The effects of seeing in the Earth's atmosphere are also probably involved. If three disks of equal size, one limb-darkened, another uniformly illuminated, and the third limb-brightened, are observed in the presence of seeing disturbances, the limb-brightened disk will appear larger, and the limb-darkened disk, smaller, than the uniformly-illuminated disk. Accurate corrections for seeing effects are not easy to make, and it is quite possible that these alone may account for much of the disagreement among the diameter measurements.

6.2 General Remarks on Observation and Analysis

Compared to stellar occultations, planetary occultations are very leisurely events (the duration of the Uranus occultation was some 16 seconds). This fact has important consequences for both observation and analysis of such events. A time resolution of 10 or even 100 milliseconds is adequate, but the observation must be prolonged over an extended interval. With such low time resolution, the event can be adequately analyzed in terms of geometric optics (i.e., diffraction can be ignored). However, the lunar background will change significantly during the extended interval of the observation.

The conversion between the temporal scale of the observation and the angular rate at which the lunar limb moves across the occulted object is critically important to the analysis of planetary occultations. For stellar occultations, this conversion usually poses no particular problems, since the shadow velocity (which expresses the relationship between the two rates, and which, for stellar events, can normally be assumed to remain constant) can be determined directly from the fringe spacing. This cannot be done for planetary occultations (or, for that matter, for events involving very large stars) since there are no fringes. For these cases, the relation between temporal and angular scale must be calculated from the apparent relative motion of the moon and the occulted object, as is done for lunar occultations involving radio sources. The topography of the lunar limb can have a major influence on the conversion, especially if the lunar limb is not moving approximately normal to itself at the location of the event. Under these circumstances, a planetary occultation may move over several kilometers of lunar limb (the Uranus occultation involved some 12 km), rather than the few tens of meters for a stellar event, and could, for example, begin by descending one slope and end by climbing another. Curvature of the mean limb also becomes appreciable over such distances, and must be allowed for in the calculations. This problem will be considered in detail at a later point in the analysis.

If the conversion has been successfully performed, the interval between contacts for the occultation directly measures the size of the occulted object. The detailed shape of the light curve provides information about the strip brightness distribution of the source. For

Uranus, the strip brightness can be further analyzed in terms of limb brightening/darkening and polar brightening: qualitatively, the slope of the central portion of the light curve depends on the limb brightening/darkening, and any asymmetry of the light curve about its center can be interpreted in terms of polar brightening.

It should be pointed out that the spatial resolution afforded by a lunar occultation of a planet is virtually undegraded by seeing effects. This characteristic is of particular significance for an object such as Uranus, and makes an occultation observation a particularly valuable means for investigating the appearance of that planet.

6.3 Observation

On several occasions during the past two years, Uranus was occulted by the moon. Unfortunately, only one of these events, the re-appearance of 10 February 1977, was visible over North America under favorable circumstances. At the time of the occultation, the third quarter (59% illuminated) moon was 31 degrees above the horizon at Prairie Observatory. The sky transparency was good, although the seeing was rather disturbed (~4"), and scintillation was quite pronounced. Telescope pointing was achieved by tracking a nearby star (5 Librae) until shortly before the time predicted for emersion, and then off-setting to the expected position of the planet. In order to minimize the chances for an unfortunate outcome to this procedure, the event was viewed through a comparatively large (24") diaphragm. This insurance was dearly paid for in terms of scattered moonlight entering the photometer, Uranus contributing only about 12% of the total light.

In fact, visual inspection after the event showed the planet to be well-centered in the diaphragm.

The spectral filter designated "NB" in Table II was used for the observation. The relative spectral response of the system (telescope optics, filters, and photomultiplier) is shown in Figure 12. The bimodal shape is due to the spectral filter. By chance, this response and the spectrum of Uranus have somewhat similar shapes in this spectral region (Elliot et al., 1977), as shown in the figure. Thus, the composite response strongly favors the continuum between the 6700 Å and the 7300 Å methane bands in the Uranian spectrum.

It was found necessary to attenuate the light (roughly by a factor of two) using a neutral density filter (the transmission of this filter turns out to be wavelength-dependent in the spectral region of the observation: the responses shown in Figure 12 include this effect). The accumulator dumps were also truncated by two bits. The observation was made over an interval of almost two minutes. Mr. William Tetley assisted in the observation.

The observational light curve is shown as Figure 13. Each of the 1792 data points of that figure represents the sum of 64 one-millisecond time frames. The abscissa is scaled in relative time units, with the origin corresponding to 9:32:00.0 UTC with an uncertainty of perhaps 1/4 second. The ordinate represents the truncated count per 64 msec time frame. The slope in the baseline is due to the gradual decrease in background light as the bright portion of the moon slowly moved away from the photometer aperture. Scintillation, in the form of increasing noise, becomes increasingly apparent as the planet emerges.

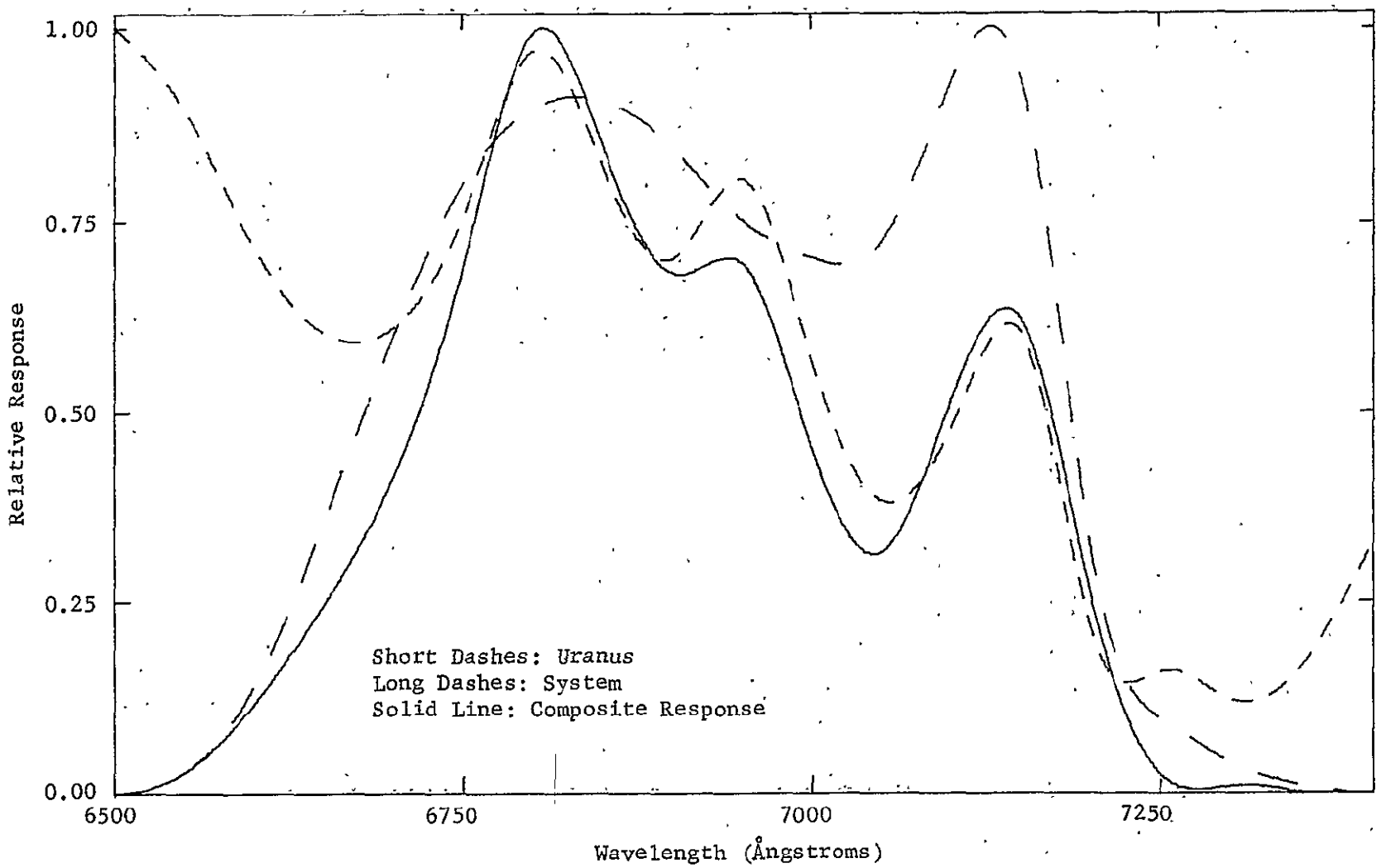

Figure 12 Relative Responses

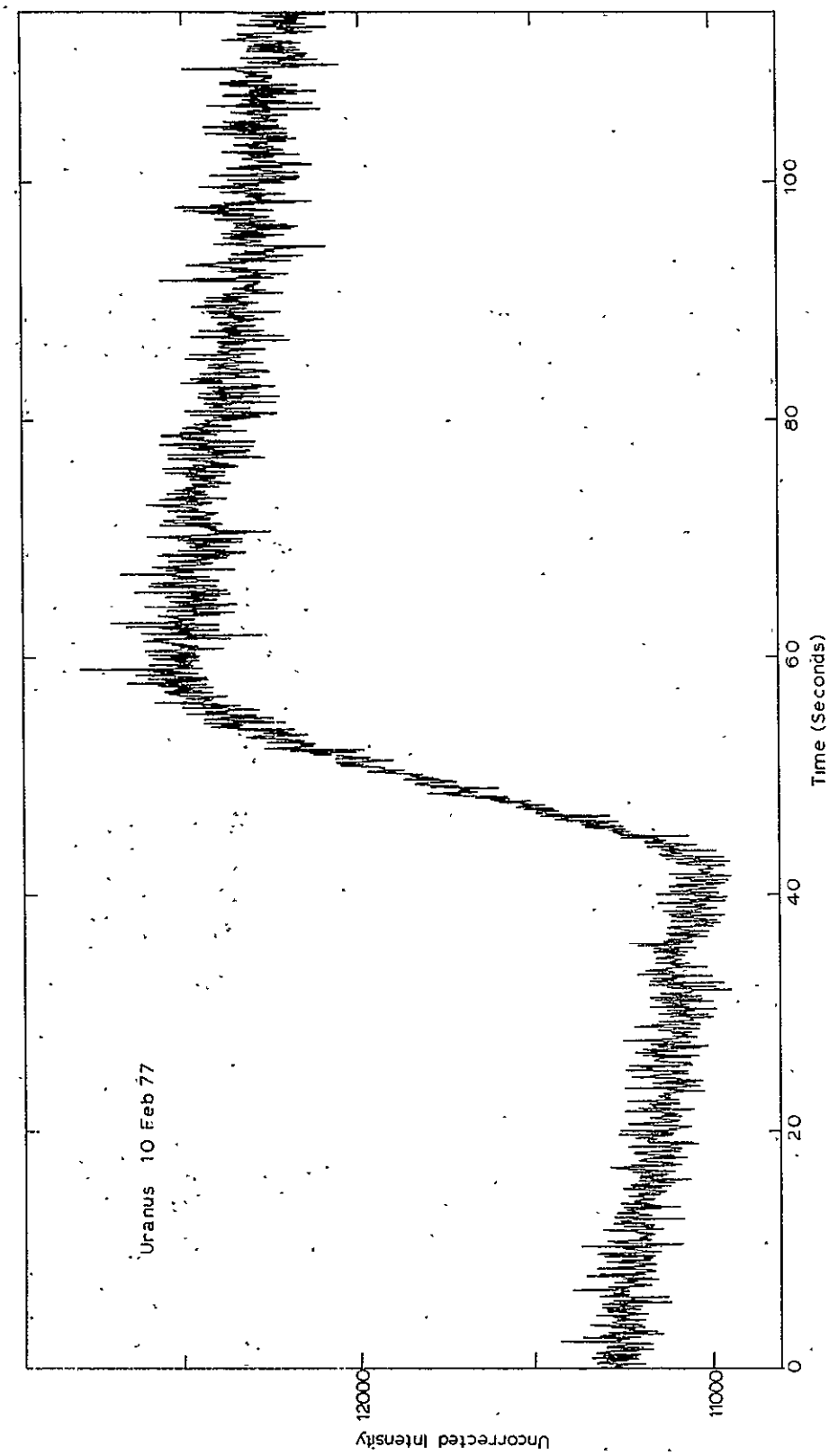

Figure 13 Observational Data, Uranus

6.4 Analysis

The procedure adopted for the analysis of these data divides itself rather naturally into four parts. The first involves the removal of the lunar background from the observational light curve, followed by a normalization. The second is the calculation of the relation between temporal and angular scale, which was discussed in general terms previously. The angular size of the planet is then derived. Finally, the corrected light curve is analyzed in terms of limb brightening/darkening and polar brightening.

6.4.1 Baseline Removal and Normalization

The lunar background was removed by fitting a segmented linear baseline to those data points which clearly lay outside the occultation itself (points 1 to 550 and 1001 to 1790) by least squares. The two segments of the baseline were constrained to share a common slope; accordingly, the difference between the intercepts measures the amplitude of the occultation. The light curve was corrected by removing a baseline with this common slope, and the ordinate scale was then re-adjusted such that the amplitude of the occultation equaled unity. Inspection of the normalized light curve reveals no features which suggest that a higher-order baseline is required. This impression was checked quantitatively by fitting the two baseline segments of the trace separately and comparing the slopes of the best-fit lines. The two slopes agree reasonably well; the intervals defined by the standard errors of the fits overlap, atlthough neither slope is included within

the error interval of the other. This result, although not wholly satisfying, does appear to indicate that higher-order baseline removal would not much alter the features of the corrected light curve.

It is unnecessary to correct the light curve for any effects due to truncation of the data. This truncation is responsible for a small portion of the noise in the normalized light curve (which cannot be corrected for, anyway), but it does not distort its scale. Similarly, no correction for coincidence losses is really necessary. Since the system bandwidth is uncertain, such correction would also be uncertain. However, even assuming a conservative 10 MHz for the system bandwidth, the correction would amount at most to 0.003 unit on the normalized scale. Subsequent calculations have demonstrated that a correction of this magnitude affects only the polar brightening analysis. However, the polar brightening is much more severely affected by uncertainties in the relation between temporal and angular rates. The comparatively small effects due to bandwidth corrections have been ignored, for these reasons. The central portion of the corrected light curve is shown in Figure 15 at the end of section 6.4.4.

6.4.2 Conversion Between Temporal and Angular Rates.

The circumstances of the occultation, as predicted by the U. S. Naval Observatory, apply only to the midpoint of the event. In order that the relationship between temporal and angular rates might be confidently calculated over the entire duration of the event, it is necessary to calculate these circumstances over the extended interval of the event. Accordingly, a computer program was written for this

purpose. Topocentric positions and distances for the centers of the moon and Uranus, librations, and the position angle of the lunar axis were calculated as functions of time for an interval of about thirty seconds, centered on the midpoint of the occultation, by interpolating the geocentric data tabulated in The American Ephemeris and Nautical Almanac, and applying the appropriate parallactic corrections. From these, topocentric values for the direction and angular rate of the apparent lunar motion relative to Uranus were derived, as well as values for the angular separation and position angle of Uranus, measured relative to the center of the moon. Limb corrections were taken from the Watts' charts (Watts, 1963; Van Flandern, 1970). Table X summarizes both the USNO predictions and the results of these calculations, both sets of figures refering to the midpoint of the occultation. The differences present among these numbers may reflect any of a variety of things: differences in the ephemerides used, interpolation round-off errors, truncation errors in computation, or differences in the precepts used for the calculations. It is probably reasonable to suppose that these differences are representative of the uncertainties in the circumstances of the occultation, namely ± 1 sec in time, and ± 0.1 degree in angle.

It is convenient to refer the geometry of the occultation to a Cartesian co-ordinate system fixed on the lunar limb, as shown in Figure 14. The origin of this system has been arbitrarily placed at WA 219.0, near the position predicted for the central re-emergence. Both axes of this system are scaled in arcseconds. Both limb curvature and elevation changes relative to the mean limb, as read from the Watts' charts,

Table X

Predicted Circumstances for Midpoint of the Uranus Occultation

Circumstance	USNO Pred	Present Pred
Time (UTC, 10Feb77)	9:32:49	9:32:50
Position Angle	238.2	238.1
Contact Angle	-126.8	-126.8
Watts' Angle	219.1	219.0
Long. Lib.	-0.3	-0.4
Lat. Lib.	-1.0	-1.0
Shadow Velocity	0.4520 km/sec	0.4524 km/sec

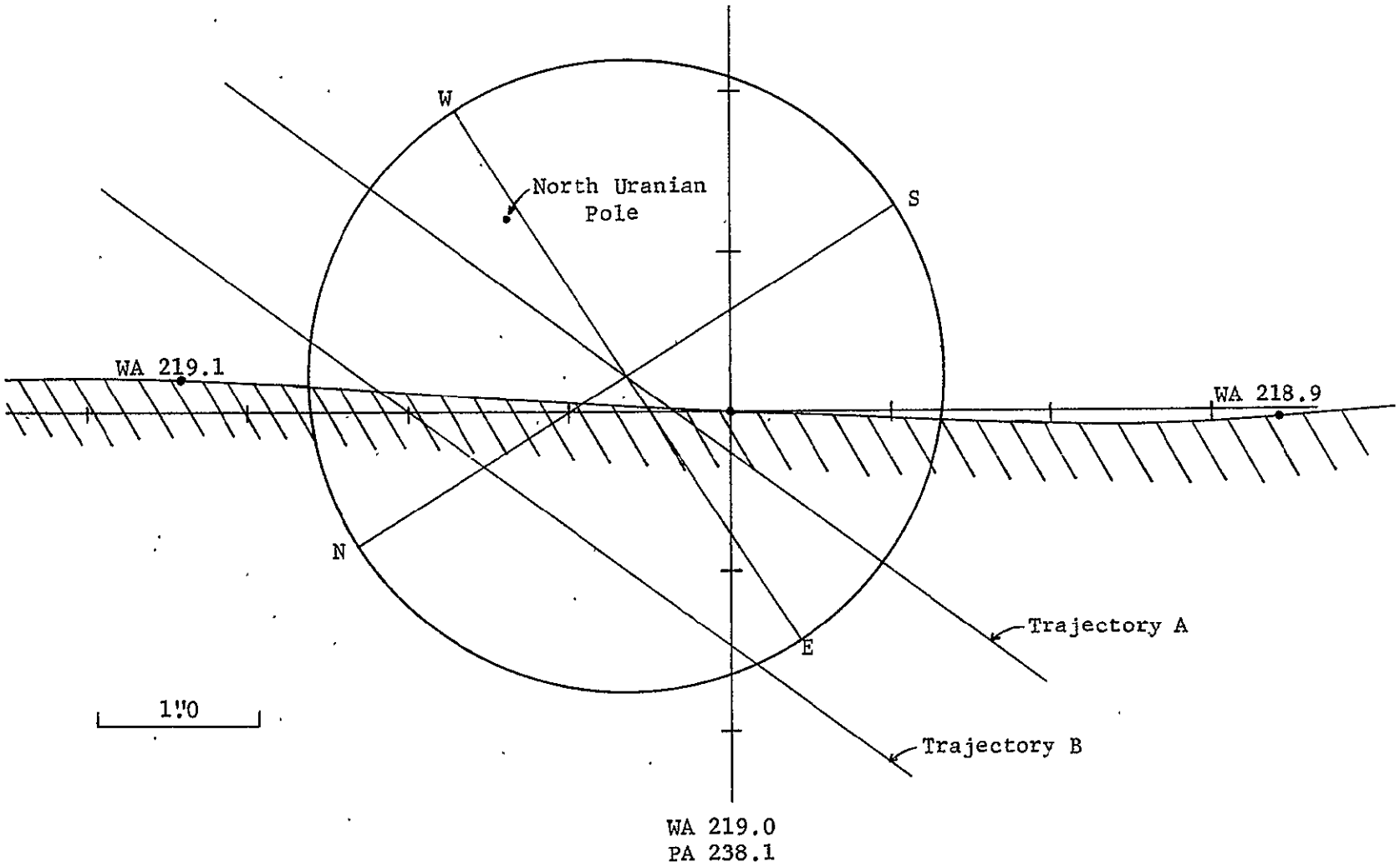

Figure 14 Geometry of the Uranus Occultation

contribute to the indicated limb contour, which was derived from a Lagrangian interpolation polynomial passed through seven points (of which only three fall within the restricted interval shown in the figure). The trajectories labeled A and B are drawn in the direction of the apparent lunar motion relative to this co-ordinate system. One may think of either the lunar limb moving down and away from Uranus, or Uranus rising above the limb, in the direction of these lines. Trajectory A is based on the circumstances predicted by the present calculation. Trajectory B differs from trajectory A by 0.1 degree in position angle (or Watts' angle), as measured around the lunar limb, and corresponds approximately to the USNO prediction. Each trajectory represents the path followed by the center of the planet relative to the lunar limb, as determined by the corresponding prediction.

For each trajectory, the angular distance between the center of the planet and the polynomial representing the lunar limb was calculated, second by second, and from these distances, the angular rate of approach (or recession), as a function of time, was derived. These rate data were then summarized by a fourth-order approximating polynomial, and the resulting formulae were used to convert the temporal scale of the occultation into angular measure. The observational time scale was related to the predicted time scale by assuming that the center of the planet reappeared at the predicted time, an assumption which would appear to be in error by at most a second or so. For trajectory A, the angular rate of the occultation slows down by some 3%, relative to a uniform temporal rate, as the event progresses. For trajectory B, the angular rate accelerates by some 2%. Some thought about the geometry of

Figure 14 indicates that this behavior is due to the relationship between the locations of the two trajectories and the hill which is present on the lunar limb.

These calculations provide the means whereby the observational trace may be compared to a model involving a straight edge moving at a uniform angular rate across the planetary disk. Unfortunately, the accuracy of the calculations does not match their numerical precision. Neither the circumstances of the occultation nor the shape of the lunar limb profile is known to sufficient accuracy to allow the calculation of a truly reliable rate conversion. Lacking this, the remaining portions of the analysis will be performed for each of the trajectories, and best values, with uncertainties, estimated somewhat informally from the two results.

6.4.3 Determination of Angular and Linear Radii

The geometry of Figure 14 and the interval between first and last contacts are sufficient to determine directly the angular size of Uranus. An impersonal determination of the contact interval is complicated by the noise in the data, and the presence of rather slow level fluctuations both before and, especially, after the occultation, which may reflect scintillation effects. Therefore, the contacts were chosen subjectively, the judgment being guided in part by use of light curves smoothed to a greater degree than the one shown in Figure 15. The contact points selected are shown in that figure. The identification of the last contact is rather uncertain; essentially, the selection was governed by the desire to smoothly approach unit

amplitude. The points selected define a contact interval of 16.17 seconds, with an estimated uncertainty of two or three percent. This interval can be converted to the angular distance, as measured along either of the trajectories in Figure 14, through which the moon moved during this interval (6.860"). If an interval of this length is laid down along one of the trajectories, such that the distances between the endpoints of the interval and the limb contour are equal, then this distance must be the angular semi-diameter of the planet. In this manner, one finds the following results:

Trajectory A s.d. = 1.95" radius = 26000 km
Trajectory B s.d. = 1.94" radius = 25800 km

If a 2% error is assumed for the contact interval, and the difference between the determinations is assumed to be indicative of the error due to geometric uncertainty, then

radius = 25900 ± 600 km

in virtual agreement with the results of Danielson et al. The 3% phase angle between the sun and the Earth, as seen from Uranus, introduces no significant error into the measurement (it is about 0.07%). The topocentric distance to Uranus (18.367 A.U.) was used to convert the angular semi-diameter into linear measure.

6.4.4 Limb Brightening/Darkening and Polar Brightening

Limb brightening/darkening was modeled using the Minnaert function (Binder and Jones, 1972; Binder and McCarthy, 1973), which states that the intensity observed at any point on the planetary disk is proportional to

$$\cos^{k}(i) \cdot \cos^{k-1}(e)$$

where i is the irradiation angle and e the emission angle for that point. The parameter k characterizes the nature of the limb brightening/darkening: assuming i = e, the disk appears limb darkened if $k > 0.5$, uniformly illuminated if $k = 0.5$, and limb brightened if $k < 0.5$. Polar brightening was incorporated into this model by means of a function $B(\phi)$, ϕ being Uranian latitude. In practice, only two such functions were considered in detail; one, $B(\phi) = 1 + B^{*}\sin(|\phi|)$, corresponds, roughly, to a "dark equatorial belt" model, whereas the second, $B(\phi) = 1 + B(1 - \cos(\phi))$, represents a "bright polar cap" model. The parameter B measures the increase in brightness at the pole relative to that at the equator, for zero phase angle. The complete models are

$$I_1 = (1 + B_1 \sin|\phi|)\cos^{k_1}(i)\cos^{k_1-1}(e)$$

and

$$I_2 = [1 + B_2(1 - \cos\phi)]\cos^{k_2}(i)\cos^{k_2-1}(e).$$

The occultation was modeled in terms of these relations by

subdividing the disk of the planet into a square grid. A particular square was considered part of the disk if its center lay inside the circular boundary of the disk. Tests demonstrated that subdivisions of fifteen and twenty-five squares/diameter yield essentially identical results; consequently, the coarser subdivision was used throughout these calculations. For each grid-square midpoint, values for the angles i, e, and ϕ were evaluated, and normalized model occultation curves calculated over a range of the parameters k and B by computing the intensity for each grid square within the disk, summing the appropriate strips, and then summing the strip brightnesses and normalizing. This procedure produced models evaluated at sixteen evenly spaced points, the two endpoints having zero and unit intensities, respectively. Continuous curves were constructed for each discrete model using cubic spline functions, the slopes of these curves being constrained to approach zero at the endpoints. These continuous models were then compared to the normalized observational trace in the sense of least-squares, the abscissa of the observational trace having been first converted to angular units using the rate relations derived previously. The best fits were identified by means of a simple grid search. The results of these calculations are summarized below. In all cases the interval of the grid search was 0.025 unit in k and 0.05 unit in B, and 253 points were fitted on the observational trace.

Trajectory A: $k(B = 0) = 0.625$
$k_1 = 0.525 \quad B_1 = 2.15$
$k_2 = 0.575 \quad B_2 = 1.75$

Trajectory B: $k(B=0) = 0.575$
$k_1 = 0.500 \quad B_1 = 2.95$
$k_2 = 0.550 \quad B_2 = 2.20$

C-2

The formal standard errors of these fitted values may be estimated by calculating the curvature of $\chi^2(k,B)$ at its minimum as a function of each parameter (Orear, 1958). Here $\chi^2 = s.s./\sigma^2$, where s.s. is the residual sum-of-squares, and σ^2, the variance for each measurement, is determined primarily by the counting statistics. The grid-search provides the values for s.s., and $\sigma^2 = 0.00122$ for the normalized data. The uncertainties so derived are

$\Delta k(B=0) = \pm 0.081$
$\Delta k = \pm 0.040$
$\Delta B = \pm 0.10$

Allowing a 2% error for the contact interval, and supposing, as before, that the uncertainty due to geometry is represented by the differences between the determinations, the indicated values for the parameters are:

$k(B=0) = 0.60 \pm 0.09$
$k_1 = 0.51 \pm 0.04 \qquad B_1 = 2.6 \pm 0.6$
$k_2 = 0.56 \pm 0.05 \qquad B_2 = 2.0 \pm 0.3$

The results of these calculations are illustrated in Figure 15, which shows the central portion of the normalized light curve and the best-fit model light curves for trajectory A, for the case B = 0 and for model 2 (the "bright polar cap" case). The asymmetry of the observational trace is clearly evident when it is compared to the symmetric model for the B = 0 case. At first sight, it is difficult to

see how the model for the B = 0 case can actually be a best-fit. It is, however, and this becomes apparent when it is noted that this curve must pass through the half-intensity point exactly midway between the contact points. The midpoint of this curve is thus fixed, and the fit can be improved on one side of the midpoint only at the price of worsening the fit on the other side. The best-fit curve for the "dark equatorial belt" model, as well as those for trajectory B, are essentially indistinguishable from the ones illustrated.

It should be pointed out that the parameter values derived here are not mutually independent. In particular, the angular diameter and limb brightening/darkening parameter are correlated. This correlation was investigated, and it was found that each 2.5% increase (or decrease) in the assumed angular size of the planet produces a corresponding increase (or decrease) of about 0.10 unit in the value of k.

6.5 Interpretation and Discussion

The results of the above analysis indicate that Uranus has a radius of some 25900 km, that it is slightly limb-darkened at 6900 Å, and that it shows pronounced polar brightening of some sort at that wavelength. How certain are these results?

They all depend on the accuracy of the calculation of the circumstances of the occultation. In particular, the derived value for the radius is particularly sensitive. If the event is moved to WA 218.9, the radius increases by some 800 km, whereas if the occultation occurred at WA 219.2, the radius decreases by about the same amount. It is fortunate that the two sets of predicted circumstances do

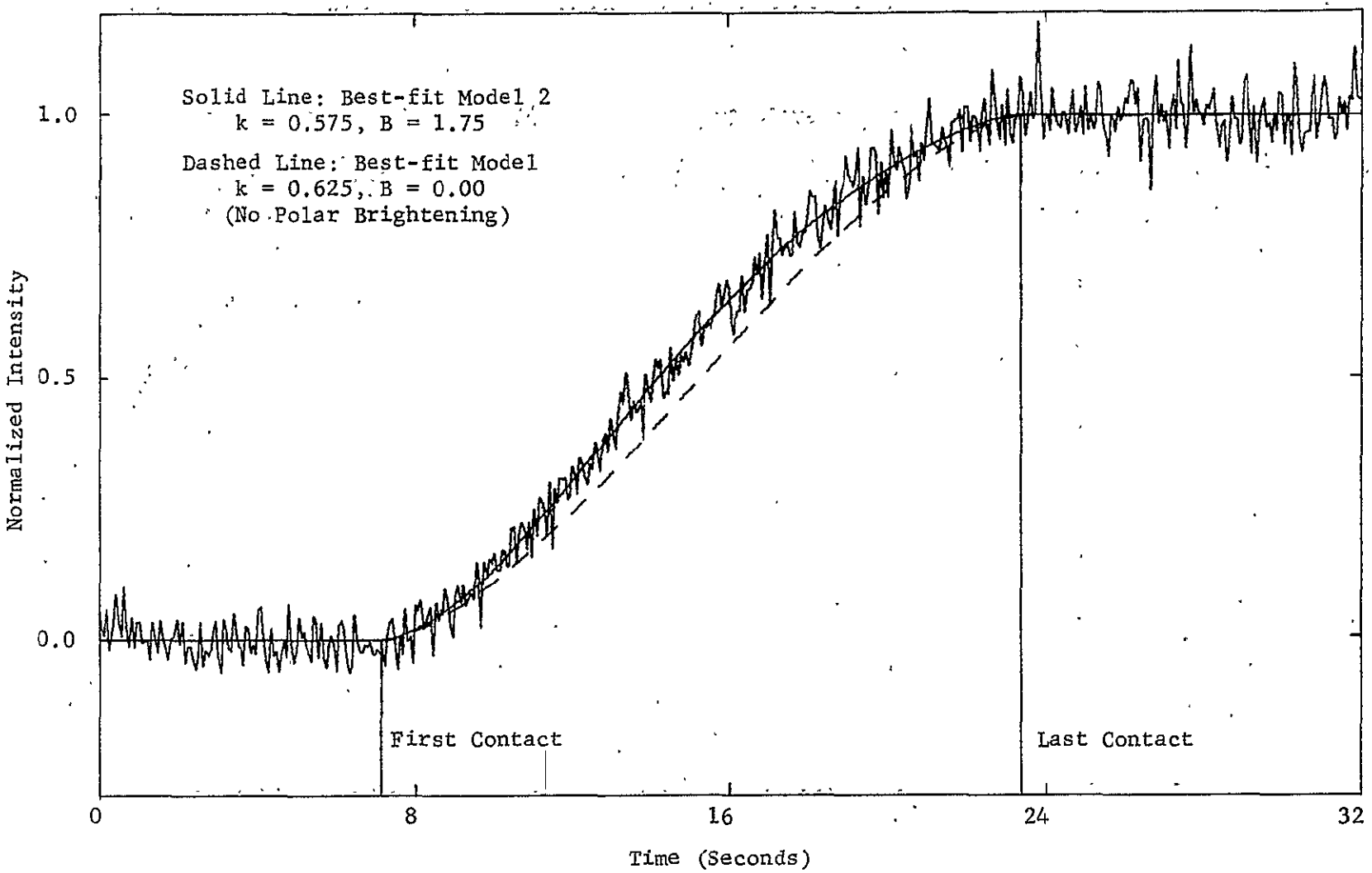

Figure 15 Fitted Data, Uranus Occultation

not produce wildly differing estimates of the planetary radius, but the island of stability is perilously small. The value of the parameter k is somewhat less sensitive in this respect, and the statement made above concerning the limb darkening is probably safe. The numerical value for the Minnaert parameter k is somewhere in the range 0.5 to 0.6 in the bandpass of the observation. Of course, it is conceivable that the Minnaert Law itself is inappropriate to describe the limb-darkening of Uranus, but this would be rather surprising in itself were it to be so. The Minnaert Law has been successfully applied to describe the appearance of a wide range of objects, including Mars, Jupiter, and Saturn (Binder and Jones, 1972; Binder and McCarthy, 1973).

The polar brightening is another matter. This characteristic depends very critically on the temporal-to-angular rate conversion, such that rather subtle differences between rate conversion formulae produce factor-of-two changes in the magnitude of the polar brightening parameter. In fact, the amount of polar brightening demanded by the models seems to be uncomfortably large. To check this impression, model brightness distributions were numerically smeared to simulate aperture and seeing effects, and used to calculate "pinhole scans," which were compared to the observations of Franz and Price (1977). Figure 16 illustrates such model scans for the best-fit "dark equatorial belt" model of trajectory A. Two scans, one along the Uranian meridian and passing through the Uranian pole, the other, passing along the Uranian equator, are illustrated. These experiments suggest that the Franz and Price observations might be consistent with a value of 0.5 or even 1.0 for the parameter B, but not a value much larger. Although one cannot

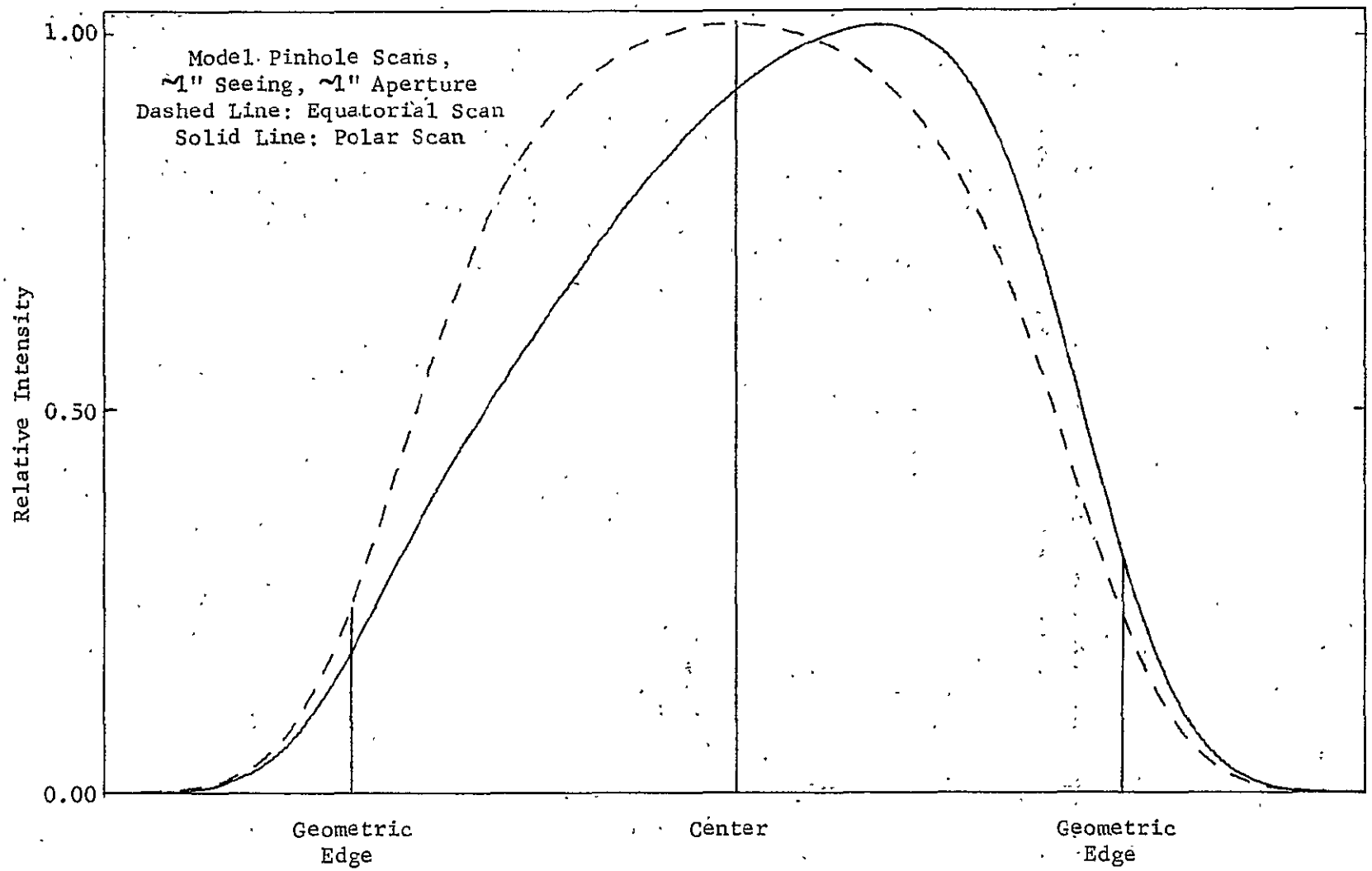
Model Pinhole Scans,
~1" Seeing, ~1" Aperture
Dashed Line: Equatorial Scan
Solid Line: Polar Scan
1.00
0.50
0.00
Relative Intensity
Geometric Edge
Center
Geometric Edge

Figure 16

dismiss completely the possibility that the larger value obtained in the above analysis is correct, it seems safest simply to conclude that the occultation observation confirms the existence of polar brightening. The fits do not distinguish between the two polar brightening "laws" considered, nor do they appear to yield a particularly reliable quantitative measure of the amount of polar brightening present on Uranus.

VII. Epilogue

7.1 General Conclusions Concerning Occultation Observations

Beyond the specific results discussed in the preceding pages of this dissertation, this research effort suggests certain conclusions of a more general nature which should also be pointed out. Principally, it demonstrates the versatility of a modern, relatively inexpensive, high-speed, computerized photoelectric photometry system. It is, of course, possible to construct a specialized system for occultation obervations which may cost less than a computerized system such as the one in use at Prairie Observatory. However, a non-specialized system based on a pulse-counting electronic system, a computer, and a mass-storage device such as a tape drive or a floppy disk can be configured to function in a variety of observing situations, of which occultation observations are but one, and perhaps even a lesser one. For this reason, a small observatory with a limited budget might still find the investment in a computerized system an attractive option, even though the initial financial outlay might be somewhat greater than that necessary for a more specialized system.

This dissertation also demonstrates that an occultation observation program, even when not pursued assiduously, can provide a handsome return on the time invested in it. This may be of particular value to a smaller observatory, which may well be heavily involved in time-intensive observing programs, since occultations provide one of the few ways for converting a few minutes of telescope time into a scientific paper, and can do so on a regular basis.

A "minimal" program, such as that implied in the previous paragraph, will, of course, concentrate on "special" events, which generally means that it is the geometric and/or photometric information made available about the occulted object which is of primary interest. If "special" events are taken to include occultations of planets, satellites, asteroids, and all stars of fourth magnitude or brighter, a typical year will include perhaps twenty such events.

If the observing program concentrates on timings, then "routine" events are also of interest. The chance discovery of multiple stars is, of course, an added dividend of such a program, but the principal objective is to obtain observations useful for lunar theory and celestial mechanics. Naturally, it is possible to combine the two types of programs by simply observing all occultations which happen to occur on the night of a "special" event.

7.2 The Future of Occultation Observations at Prairie Observatory

What, then, might be a reasonable program of occultation observations for Prairie Observatory? It seems reasonable that the present concentration on "special" events be continued, considering the productivity of such observations. However, such observations would be of much greater value if performed in two colors, simultaneously, rather than in the present single-channel mode. Two-color observations permit the separation of effects due to limb structure from those due to source geometry. More importantly, if the colors selected are standard, such as the Strömgren "b" and "y" bandpasses, occultation observations of binary stars can provide accurate magnitudes and colors for the

components, information which may be available in no other way.

In fact, instrumentation for two-channel observations already exists at Prairie Observatory, in the form of a two-channel photometer, originally designed for another purpose, located at the Coudé focus of the telescope. The necessary electronics also exist. This photometer has proven to be rather awkward to use, but the advantages to be gained from two-color observation of occultations justify an attempt to use it for this purpose.

The data rate of the present system is limited by the tape drive to one kilobyte/sec. This is also the rate at which a single observing channel, operating with one millisecond time resolution, acquires data. Thus, dual-channel operation would require a reduction in the time resolution to two milliseconds. However, this represents no real loss in information, as is made apparent by the constraints presented in Section II. In fact, one millisecond observation "over-resolves" the measurement by at least a factor of two, when compared to the minimum angular resolution imposed by a one-meter aperture and the Strömgren filters. For most applications, two millisecond time resolution should be perfectly acceptable.

An exception to this might be observations involving resolvable stars. Such stars are generally red, and, since the Coudé system is not equipped with red-sensitive photodetectors, such observations are probably best made in the present single-channel mode, using the red-sensitive Cassegrain photometer.

One aspect of "routine" observations, the timing of reappearances, is also particularly attractive for Prairie Observatory. Judging from

the recent literature, occultation observers are attaching considerable importance to such obervations, but have not been particularly successful in obtaining them. The problem is, of course, that the smaller telescopes normally used for occultation observations do not normally possess drive systems which permit blind pointing. This is (with some qualification) not the case with the telescope at Prairie Observatory, which has a sophisticated digital drive system. Several attempts were made over the past year to demonstrate the ability to observe reappearances using the off-setting technique described in the discussion of the observation of the Uranus occultation. Several of these attempts were clouded out, and one dramatic failure emphasized the need to correct for differential refraction. However, the 30Oct77 observation of V Taurii was undertaken with the specific goal of observing a difficult reappearance, and it succeeded. These experiments suggest that there is no reason why blind pointing accurate to one or two arcseconds in each co-ordinate cannot be achieved using this telescope, and accuracy of that order is adequate for routine observation of occultation reappearances. Of course, the capability of observing reappearances also effectively doubles the number of "special" events which are observable, but reappearance timings alone would be observations of considerable value to astronomy. A deliberate effort should be made to exploit this unique capability in any program for observing lunar occultations undertaken at Prairie Observatory.

References

Abt, H.A., and Biggs, E.S. (1972). Bibliography of Stellar Radial Velocities (Latham Process Corp., New York).

Africano, J.L., Evans, D.S., Fekel, F.C., and Ferland, G.J. (1976). Photoelectric measurements of lunar occultations. VIII Astron. J. 81, 650-658.

Africano, J.L., Evans, D.S., Fekel, F.C., and Montemayor, T. (1977). Photoelectric observations of lunar occultations. IX Astron. J. 82, 631-639.

Africano, J.L., and Montemayor, T. (1977). Approach to systematic observation of occultation reappearances Astron. J. 82, 640-641.

Allen, C.W. (1973). Astrophysical Quantities, 3rd edn. (Althone Press, London).

American Ephemeris and Nautical Almanac, The (1977). (U. S. Government Printing Office, Washington).

Barnes, T.G., and Evans, D.S. (1976). Stellar angular diameters and visual surface brightnesses - I Mon. Not. R. Astr. Soc. 174, 489-502.

Batten, A.H. (1967). Sixth catalogue of the orbital elements of spectroscopic binary systems Pub. Dom. Astrophys. Obs. 13, 119-251.

Becker, S.A., Iben, I., and Tuggle, R.S. (1977). On the frequency-period distribution of Cepheid variables in galaxies in the local group Astrophys. J. 218, 633-653.

Binder, A.B., and Jones, J.C. (1972). Spectrophotometric studies of the photometric function, composition, and distribution of the surface materials of Mars J. Geophys. Res. 77, 3005-3020.

Binder, A.B., and McCarthy, D.W. (1973). IR spectrophotometry of Jupiter and Saturn Astron. J. 78, 939-950.

Blanco, V.M., Demers, S., Douglass, G.G., and Fitzgerald, M.P. (1968). Photoelectric Catalogue Pub. U. S. Naval Obs. 21.

Blazit, A., Bonneau, D., Koechlin, L., and Labeyrie, A. (1977). The digital speckle interferometer: preliminary results on 59 stars and 3C 273 Astrophys. J. 214, L79-L84.

Born, M., and Wolf, E. (1970). Principles of Optics (Pergamon Press, New York).

Brown, R.H. (1968). Measurement of stellar diameters Ann. Rev. Astron. Astrophys. 6, 13-38.

Chauvenet, W. (1868). A Manual of Spherical and Practical Astronomy, vol I (Lippincott, Philadelphia).

Cousins, A.W.J., and Guelke, R. (1953). Photoelectric observation of occultations at the Cape Observatory Mon. Not. R. Astr. Soc. 113, 776-780.

Crawford, D.L., and Barnes, J.V. (1970). Standard stars for uvby photometry Astron. J. 75, 978-998.

Danielson, R.E., Tomasko, M.G., and Savage, B.D. (1972). High-resolution imagery of Uranus obtained by Stratoscope II Astrophys. J. 178, 887-900.

Draper, N.R., and Smith, H. (1966). Applied Regression Analysis (Wiley, New York).

Dunham, D.W., Evans, D.S., McGraw, J.T., Sandmann, W.H., and Wells, D.C. (1973). Photoelectric measurement of lunar occultation VI. Further observational results Astron. J. 78, 482-490.

Eddington, A.S. (1909). Note on Major MacMahon's paper "On the determination of the apparent diameter of a fixed star" Mon. Not. R. Astr. Soc. 69, 178-180.

Eitter, J.J., and Beavers, W.J. (1974). Lunar occultation summary. Astrophys. J. Suppl. Ser. 28, 405-412.

Elliot, J.L., Veverka, J., and Millis, R.L. (1977). Uranus occults SAO 158687 Nature 265, 609-611.

Evans, D.S. (1951). The occultation of Antares of 1950 June 27-28 Mon. Not. R. Astr. Soc. 111, 64-74.

Evans, D.S. (1970). Photoelectric measurement of lunar occultations. III. Lunar limb effects Astron. J. 75, 589-599.

Evans, D.S. (1977). Photoelectric observing of occultations-I Sky and Telescope 54, 164-166.

Evans, D.S., Heydenrych, J.C.R., and VanWyk, J.D.N. (1954). Observations of occultations of Antares with the Radcliffe reflector Mon. Not. R. Astr. Soc. 113, 781-785.

Fekel, F.C. (1978). Private communication.

Franz, O.G., and Price, M.J. (1977). Uranus: limb and polar brightening at 7300 Å Astrophys. J. 214, L145-L146.

Hoffleit, D. (1964). Catalogue of Bright Stars 3rd rev. edn. (Yale U., New Haven).

Jeffers, H.M., van den Bos, W.H., and Greeby, F.M. (1963). Index catalogue of visual double stars 1961.0 (IDS) Pub. Lick Obs. 21.

Jenkins, L.F. (1952). General Catalogue of Stellar Parallaxes (Yale U. Obs.).

Krishnan, T. (1970). The effects of filters and colour on stellar occultations and appropriate deconvolution procedures Highlights of Astronomy, vol. 2, 646-661 (D. Reidel, Dordrecht).

MacMahon, P.A. (1909). On the determination of the apparent diameter of a fixed star Mon. Not. R. Astr. Soc. 69, 126-127.

McCants, M.M., and Nather, R.E. (1970). Analysis of lunar occultation data Highlights of Astronomy, vol. 2, 669-674 (D Reidel, Dordrecht).

Morbey, C.L. (1972). Catalogue of theoretical lunar-occultation diffraction patterns for single and double stars occulted by the lunar limb Pub. Dom. Astrophys. Obs. 14, 45-58.

Murdin, P. (1971). Effect upon occultations of lunar surface structure along the line of sight Astrophys. J. 169, 615-616.

Nather, R.E., and Evans, D.S. (1970). Photoelectric measurement of lunar occultations. I. The process Astron. J. 75, 575-582.

Nelson, M.R. (1975). The Angular Diameter of Mu Geminorum Astrophys. J. 198, 127-129.

O'Keefe, S.A., and Anderson, J.P. (1952). The Earth's equatorial radius and the distance to the moon Astron. J. 57, 108-121.

Orear, J. (1958). Notes on Statistics for Physicists (Univ. of California Radiation Lab., Berkeley).

Ptolemy, C. The Almagest.

Ridgway, S.T. (1977). Considerations for the application of the lunar occultation technique Astron. J. 82, 511-515.

Ridgway, S.T., Wells, D.C., and Joyce, R.R. (1977). Angular diameters for 11 late-type stars by the lunar occultation technique Astron. J. 82, 414-430.

Sanford, R.F. (1939). Spectrographic elements for β Capricorni Astrophys. J. 89, 333-346.

Scheuer, P.A.G. (1962). On the use of lunar occultations for investigating the angular structure of radio sources Australian J. Phys. 15, 333-343.

Schlosser, W., Pansch, E., and de Vegt, Chr. (1970). Ein lichtelektrishes Photometer zur Registrierung on Sternbedeckungen Astr. Astrophys. 8, 85-92.

Sinton, W.M. (1972). Limb and polar brightening of Uranus at 8870 Å Astrophys. J. 176, L131-L133.

Smith, B.A. (1977). Uranus photography in the 890-nm absorption band of methane Bull. Amer. Astron. Soc. 9, 744-745.

Stokes, N.R.R. (1972). Four-colour and H photometry of some bright southern stars-II Mon. Not. R. Astr. Soc. 160, 155-168.

Van Flandern, T.C. 1970). Some notes on the use of the Watts limb-correction charts Astron. J. 75, 744-746.

Watts, C.B. (1963). The marginal zone of the moon Astron. Papers Am. Ephem. 17.

Whitford, A.G. (1939). Photoelectric observation of diffraction at the moon's limb Astrophys. J. 89, 472-481.

Whitford, A.G. (1946). Angular diameters of stars from occultations by the moon Astron. J. 52, 131-132.

Williams, J.D. (1939). A method for the determination of stellar diameters Astrophys. J. 89, 467-471.

Vita

Richard Raeburn Radick was born [redacted], in [redacted], [redacted]. After graduating as class valedictorian from Fulda Public High School, he entered the University of Minnesota, Morris Campus, Morris, Minnesota, receiving a Bachelor of Arts degree with Highest Distinction in 1969. He spent the next two years in military service with the U. S. Air Force and teaching high school mathematics in Aberdeen, Mississippi. In 1971 he entered Rensselaer Polytechnic Institute, Troy, New York, receiving a Master of Science degree in astronomy in 1973. While at Rensselaer Polytechnic Institute, he was a laboratory instructor in both physics and astronomy, and received a departmental citation for distinguished teaching in 1973. He entered the Graduate School in astronomy at the University of Illinois, Urbana, Illinois, in 1973, and held both teaching and research assistantships, as well as a University Fellowship, during his studies there. He was elected to the Honor Society of Phi Kappa Phi in 1978.